Fermi National Accelerator Laboratory

FERMILAB-Pub-86/33
0102.000
1111.000

ENERGY LOSS AND ANGULAR CHARACTERISTICS OF HIGH ENERGY ELECTROMAGNETIC PROCESSES*

A. Van Ginneken

February 1986

*Submitted to Nucl. Instrum. Methods A

Operated by Universities Research Association Inc. under contract with the United States Department of Energy

ENERGY LOSS AND ANGULAR CHARACTERISTICS OF HIGH ENERGY ELECTROMAGNETIC PROCESSES

A. Van Ginneken

Fermi National Accelerator Laboratory
P.O. Box 500, Batavia, IL, 60510.

February, 1986

ABSTRACT

For high energy protons, pions and muons (up to 30 TeV) the energy and angle of the final state particles in bremsstrahlung, direct pair production and, for muons, deep inelastic scattering are determined as a function of the fractional energy loss of the incident particle. The results are parametrized for convenient use in Monte Carlo simulations. The average energy loss and rms angular deflection of muons, pions and protons in bulk matter are determined and compared with other work.

1. Introduction

The design of the Superconducting SuperCollider [1] (SSC) with its contemplated 20 TeV proton beams poses certain problems concerning shielding, target heating, etc. Such problems are typically analyzed via the Monte Carlo (MC) method by simulating the propagation of high energy cascades in bulk matter. To extend the valid energy range of such codes into the SSC realm the basic processes of particle production and transport must be re-examined at these higher energies.

One striking feature of the TeV regime, with respect to particle transport, is that with increasing energy bremsstrahlung begins to dominate multiple Coulomb scattering as a source of angular diffusion. Likewise even for heavy ($>>m_e$) particles direct pair production as well as bremsstrahlung become more important than ionization as a source of energy loss in transport.

This paper presents some calculated results on the angular and energy distributions resulting from bremsstrahlung, direct pair production and muon inelastic scattering. These results are cast into a form convenient for implementation into the MC code CASIM [2]. Obviously, this may also serve other codes and carry some more general interest as well. It must be pointed out that CASIM is a weighted transport code in which essentially only one of the outgoing particles from each interaction is followed. This means that correlations among the final state particles may be neglected. Considerably more work is needed to simulate complete events as is required in analog MC transport codes.

Specifically the information presented here aims at two areas of interest to high energy transport. The first is the calculation of the maximum energy deposited in a thick target. At 20 TeV beams are smaller and angular deflections are smaller leading to large energy densities where beam is dumped either intentionally or accidentally. Therefore one needs algorithms capable of simulating the spatial distribution of energy deposition over radial distances well within a beam diameter (as low as 50 μm). The second application concerns muon transport. Muons in the TeV regime exhibit a broad "range straggling" distribution. This means that the dimensions of a muon shield are no longer determined by simple considerations of range plus multiple Coulomb scattering but require instead the detailed (radial and longitudinal) behavior of the radiation dose in the straggling tail. The radial distribution is significantly affected by the angular deflections from bremsstrahlung and inelastic scattering off nuclear targets.

Algorithms for multiple elastic scattering are not discussed here. Improvements have recently been introduced into CASIM using a two component approach. Below a judiciously chosen cut-off angle it is treated in the Gaussian approximation. Above this angle it is treated event-by-event using predictions of Glauber [3]. This will be documented separately.

In the course of calculating the distributions in energy and angle of the particle undergoing these processes the stopping power (dE/dx) for the various processes is easily obtained. This provides a gross check on the present calculations as well as a set of dE/dx values in principle more accurate than those available from analytical formulae by virtue of the inclusion of form factors, more precise kinematical treatment, etc.

The present study is limited to muons, pions and protons as incident particles with energies between 3 GeV and 30 TeV. Electrons and photons in the TeV regime require more care since certain corrections need be applied for energies above ~ 100 GeV [4]. (Similar corrections for muons or heavier particles may still be ignored in the SSC regime since they scale with mass to a power unity or larger.) Messel and Crawford [5] describe the application of such corrections to electromagnetic showers but their treatment is limited to the effects on total cross sections and on $d\sigma/dE$. They do not consider angular diffusion due to processes other than multiple Coulomb scattering.

Next, the implementation of the present work into the MC code CASIM is briefly indicated so as to motivate the following sections which in turn discuss bremsstrahlung, direct pair production and muon inelastic scattering. In the last section results on the stopping powers and rms angular dispersions in bulk matter of the various processes are presented along with a limited comparison with other work.

2. Implementation into Monte Carlo

CASIM traces the particles of a shower stepwise through the problem geometry. For each such step and for each process the average number of interactions is obtained from its total cross section. Based on this the (randomly variable) number of interactions in a particular step is chosen from a Poisson distribution. For all bremsstrahlung processes the total cross section is restricted to events with energy losses in excess of 1 MeV. In the energy range where bremsstrahlung is significant

the average energy loss due to sub-MeV photons is negligible. While screening by atomic electrons actually removes the infrared divergence at very low energies, inclusion of these soft photons in a MC would consume considerable computer time.

For each simulated interaction the energy of the final state of the incident particle is randomly selected from the distribution function $\sigma^{-1}(d\sigma/dv)$, where $v=(E-E')/(E-m)$ is the fractional energy loss $(0< v <1)$. Next the angular deflection is chosen. The main simplification occurs in this step viz., the rms (spatial) angle, $\langle\theta_2^2\rangle^{1/2}$, between incident and outgoing particles is determined and a specific angle is chosen assuming the projected angles θ_x, θ_y follow a Gaussian distribution with zero mean and $\sigma^2=\langle\theta_2^2\rangle/2$. (Equivalently the spatial angle may be chosen from an exponential in the variable θ_2^2 with mean $\langle\theta_2^2\rangle$ and $\sigma^2=\langle\theta_2^2\rangle$).

In all of the processes under study there is a strong positive correlation between $\langle\theta_2^2\rangle^{1/2}$ and energy loss and it is important that this correlation be kept in the simulation of all applications where angular diffusion from these processes is significant. For example, in muon transport this influences the radial distribution at large depths since the more penetrating muons are also better collimated.

Although the angular distributions for a fixed outgoing energy are not explicitly calculated here, it is unlikely that they much resemble Gaussians. The rationale for this approximation rests with the Central Limit Theorem which is similarly invoked in the case of multiple Coulomb scattering to go from (single) Rutherford scattering to a Gaussian. The often

voiced criticism [6] in the latter application is that for insufficiently thick targets the tail of the single scatterings exceeds the Gaussian at large angles. This criticism may also be applied to the present use of the theorem since a typical step in a MC simulation is, by this standard, not a thick target. But the criticism can be somewhat mitigated if it is understood that a program like CASIM does not aim to reproduce single events but only an average over many events.

Consider then the ideal case of a mono-energetic pencil beam incident on a slab of finite thickness. In contrast with multiple Coulomb scattering the angular distribution predicted to emerge is not a single Gaussian but a rather complicated summation over a set of Gaussians (each with its own σ). For a wide variety of conditions one might expect the larger σ's to dominate the tails of the smaller σ distributions. Hence only the tails of the largest σ single events would appear improperly simulated. Consider further that in more realistic problems additional smearing is expected e.g., the muons in a shielding calculation typically emerge from a hadron cascade taking place in a complex geometry. Nonetheless while the Gaussian approximation appears justifiable in typical applications its limitations must be kept in mind. The angular selection scheme also implies the small angle approximation. When $\langle\theta_2^2\rangle^{1/2}$ approaches or exceeds unity it is more accurate to select from an isotropic distribution.

Simulation of the energy loss and angular distribution of the incident particle for each process in the above manner is sufficient for the muon problem. For the maximum energy density problem one needs also to include the other outgoing particles (i.e., γ in bremsstrahlung, e^+e^- in pair production and

target recoil). Their simulation is along the same lines as for the incident particle, though in the case of pair production it is more complicated. Conservation of energy and momentum permit in some cases a simplification of the prescription. Simulation of the hadron shower initiated by muons is not considered here. For most such problems the objective is estimating muon fluxes rather than energy deposition. Where it is explicitly required it is usually reasonable, in view of their deep penetration, to deposit all muon energy losses locally along their trajectories.

The next three sections describe for each of the processes what is specifically needed for a CASIM-type simulation and how it is calculated. Duplication of the (often lengthy) cross-section formulae from the various sources is avoided but an attempt is made to adhere to their notation. The results of the calculation are then presented as relatively simple formulae suitable for inclusion in a MC calculation. In particular, the $\sigma^{-1}d\sigma/dv$ are cast in a form from which it is easy to sample. The parametrizations are explicitly provided for their possible implementation elsewhere. These formulae are simply fits without necessarily any physical significance and they should not be used outside the 3 GeV- 30 TeV range without further checking. If a particular application permits it, the parametrizations may be further simplified for economy of computation. The many illustrations which compare the fits with direct calculation aim also to provide a general impression of the energy loss distributions and rms angles in this energy range. In all the parametrizations presented below energies and masses are expressed in GeV.

3. Bremsstrahlung

3.1. Calculation

The differential cross section for bremsstrahlung in lowest order Born approximation is presented by Mo and Tsai [7] in the form $d\sigma/dpd\Omega$, where p and Ω are respectively the momentum and solid angle of the particle after photon emission. In particular, the cross section is expressed as an integral over θ_k and ϕ_k, the polar and azimuthal angle between the photon and $\vec{P}-\vec{p}$, the difference between incident and outgoing momentum. Also in ref. 7, the integration over ϕ_k is performed analytically leaving a single integral over θ_k. The expression includes the kinematics of target recoil but does not include photon emission by the target.

Four different contributions are evaluated using the Mo-Tsai formula: (i) coherent nuclear bremsstrahlung, (ii) incoherent bremsstrahlung off individual nucleons as well as (iii) off atomic electrons, (iv) photons emitted by recoiling electrons. For hadron targets (and/or projectiles) there is also a deep inelastic contribution to the bremsstrahlung whereby pions, etc. are produced along with the photon. (In contrast, (ii) refers to the quasi-elastic component.) For incident hadrons this process resembles an inelastic hadronic interaction but is negligible in comparison. For incident muons it is included as a radiative correction. Deep inelastic scattering of hadrons off atomic electrons is dealt with elsewhere [8].

The information required to perform the simulation includes $\sigma^{-1}(d\sigma/dv)$ and $\langle\theta_2^2\rangle^{1/2}$ as a function of v. For incident hadrons the v-dependence of $\langle E_\gamma\rangle$ and $\langle\theta_\gamma^2\rangle^{1/2}$, the average photon energy and rms angle, as well as $\langle T_R\rangle$ and $\langle\theta_R^2\rangle^{1/2}$, the average kinetic energy and rms angle of recoil are also needed.

For contributions (i)-(iii) the Mo-Tsai distribution is numerically integrated with inclusion of the appropriate form factors. For the photon angle this averaging should be carried out over ϕ_k as well. This is done in two ways: (a) by analytically integrating

$$\langle Pk \rangle = \int_0^{2\pi} (Pk)\,(d\sigma/dpd\Omega dcos\theta_k d\phi_k)\,d\phi_k \qquad (1)$$

an averaged value of Pk, the four momentum product of incident particle and photon averaged (over ϕ_k), is obtained. This is related to the angular variables, e.g.,

$$\sin^2(\theta_\gamma/2) = (|\vec{P}|-E+\langle Pk \rangle/E_\gamma)/2|\vec{P}| \qquad (2)$$

wherein $\langle Pk \rangle$ appears linearly which insures proper averaging of θ_γ (in the small angle approximation). Alternatively, (b) Pk is evaluated at ϕ_k=0. This corresponds to the peaking approximation which assumes that the photon aligns itself with either the incident or outgoing particle. Results from method (a) are practically identical with those from (b).

The form factors used are in all cases very simple. For process (i) the nuclear form factor is of the type: $(1+|t|/D)^{-2}$ with $D=0.164A^{-2/3}$ GeV^2 and t is the square of the four momentum transfer [9]. The elastic atomic form factor (screening) used is of the Thomas-Fermi-Moliere type [10]. For process (ii) the quasi-elastic form factor is taken to be the product of the nucleon dipole form factor [11] and a Pauli suppression factor. For the latter two forms are used (a) the well known overlap of two Fermi spheres and (b) a slight generalization thereof which demands a minimum momentum transfer to overcome the gap between the nuclear ground state and lowest lying

excited state. While (a) predicts a much larger contribution than (b) even the former is sufficiently small so that incoherent processes may be ignored compared with the others in the problems of interest here. For process (iii) an inelastic atomic form factor of the type proposed by Tsai [9] is used: $a^4t^2/(1+a^2|t|^2)$ with $a=1.42\cdot10^5Z^{-2/3}$ GeV^{-1}.

For process (iv) i.e., bremsstrahlung by recoiling atomic electrons, the Mo-Tsai formula is evaluated in the projectile's restframe. The energy loss of the projectile in the lab (e^- restframe), separated into photon energy and recoil, is invariantly expressed as:

$$E-E' = Pk/m_e+(Pp-m_e^2)/m_e \qquad (3)$$

where P,p are the four momenta of incident and outgoing electron. Since Pk depends on ϕ_k it is replaced by <Pk> as in the evaluation of $\langle\theta_\gamma^2\rangle^{1/2}$. To obtain $\sigma^{-1}d\sigma/dv$ for this case (where v is to the energy loss of the projectile in the lab) the differential cross section $d\sigma/dpd\Omega d\cos\theta_k$ for the electron in the projectile restframe along with the average value (over ϕ_k) of $v(\equiv\bar{v})$ is calculated on a relatively dense set of $p,\theta,\cos\theta_k$. At each point the quasi-infinitesimal contribution $(d\sigma/dpd\Omega d\cos\theta_k)(\Delta p\Delta\Omega\Delta\cos\theta_k)$ is redistributed over a set of logarithmically spaced v-bins. For each contribution v is limited between $v_{min}(\phi_k=0)$ and $v_{max}(\phi_k=\pi)$ and is assumed to be distributed as:

$$p(v) \propto \exp[-(v-v_{min})/(\bar{v}-v_{min})] \qquad (4).$$

In this manner a smooth $\sigma^{-1}d\sigma/dv$ is obtained. The convenience of this procedure vis-a-vis a straightforward change of variables is that $d\sigma/dpd\Omega d\cos\theta_k$ can be evaluated in the same fashion as for processes (i)-(iii). This requires special attention to accuracy

since (a) large cancellations occur in the Mo-Tsai formula and (b) it must be ensured that the peak regions are adequately sampled in the integration procedure. Computation of $\langle \epsilon_\gamma \rangle$, $\langle T_R \rangle$, $\langle \theta_\gamma^2 \rangle$ and $\langle \theta_R^2 \rangle$ as a function of v follows the same routine. The same inelastic atomic form factor is applied at the electron vertex as in (iii).

The two contributions to bremsstrahlung off atomic electrons are added incoherently. This is mainly for simplicity but it is supported by the rather large differences observed in the average values of corresponding kinematical variables evaluated for each process. It also appears reasonable in the framework of the peaking approximation.

Process (iv) is closely linked to certain diagrams usually dealt with as radiative corrections to elastic electron scattering. Their contributions may be evaluated using the formulae of Tsai [7,12]. These diagrams may be divided into purely elastic (where all photons are virtual) and inelastic (containing an infrared photon). The latter may be subdivided into projectile and target bremsstrahlung and their interference. In line with the last paragraph the interference terms are ignored. The infrared terms then constitute small corrections to processes (iii) and (iv). The main contribution comes from the purely elastic part. Below about 100 GeV this term is larger than the contribution of process (iv) and negative. At higher energies process (iv) becomes progressively dominant. Some illustrations of this are shown in the final section on dE/dx in bulk matter.

In a MC calculation it is the most logical to treat processes (iii) and (iv) as distinct because the above mentioned kinematical differences make separate parametrizations more

convenient. The radiative corrections to the elastic part belong in the treatment of energy loss by collision and multiple Coulomb scattering.

Certain corrections apply to the Mo and Tsai results in general, most notably the Coulomb and high frequency limit corrections. As given in the literature [13] they apply only to $d\sigma/dE$. When applied uniformly at all angles to $d\sigma/dEd\Omega$ they do not significantly alter the results and are therefore omitted altogether.

3.2. Results

The probability for photon emission off a nuclear target as a function of v is well represented by:

$$\begin{aligned} \sigma^{-1}d\sigma/dv &= k_1 v^{-1} && v_{min} < v < 0.03 \\ &= k_2 v^{-m} && 0.03 < v < v_2 \\ &= k_3 (1-v)^n && v_2 < v < 1 \end{aligned} \qquad (5).$$

The k_i are fixed by continuity and normalization, m and n depend on particle type: $m_\mu = m_\pi = 1.39 - 0.024\ln E$, $m_p = 1.99 - 0.077\ln E$, $n_\mu = n_\pi = 1.32 - 0.12\ln E$, $n_p = 2.37 - 0.18\ln E$, $v_{min} = 0.001/E$, $v_2 = E^c/(E^c+d)$ with $c_j = 0.5(m_\mu/m_j)^{1/2}$ for $j = \mu, \pi, p$, $d_\mu = d_\pi = 4.5$ and $d_p = 2.3$. A slight Z dependence in $\sigma^{-1}d\sigma/dv$ is ignored. For values of v above 0.995 the parametrization is not very reliable. This is also the regime where the high frequency limit correction may be important. For most applications these uncertainties will matter very little. Fig. 1 shows a comparison of directly calculated $\sigma^{-1}d\sigma/dv$ and the parametrization of eq. (5) for 100 GeV μ, 10 TeV μ and 20 TeV p

on beryllium and lead targets. The incoherent contribution for 20 TeV p on beryllium is also shown in the form $\sigma_{coh}^{-1} d\sigma_{inc}/dv$ for direct comparison. For lead the incoherent process is of even lesser importance.

The rms angle of the radiating particle is parametrized as:

$$\begin{aligned} \langle\theta_2^2\rangle^{1/2} &= [(k_1 v^{1/2}, k_2)_{min}, k_3 v]_{max} && v \leq 0.5 \\ &= k_4 v^{1+n}(1-v)^{-n} && \langle\theta_2^2\rangle^{1/2} < 0.2,\ v > 0.5 \\ &= k_5 (1-v)^{-1/2} && \langle\theta_2^2\rangle^{1/2} \geq 0.2,\ v > 0.5 \end{aligned} \qquad (6)$$

where $k_1^{\mu,\pi}=0.092E^{-1/3}$, $k_1^p=0.245E^{-1/2}$, $k_3=a_1E^{-0.92}$ with $a_\mu=0.220$, $a_\pi=0.275$, $a_p=1.28$ and $k_4^\mu=0.26E^{-0.91}$, $k_4^\pi=0.32E^{-0.91}$, $k_4^p=0.86E^{-0.85}$, $n=0.81E^m/(E^m+d)$ with $m_\mu=m_\pi=1/2$, $m_p=1/3$, $d_{\mu,\pi}=1.8$, $d_p=2$ and k_5^i is related to k_4^i by continuity. All the above parameters are independent of Z. But k_2 is not: $k_2=b_1E^{-1}Z^{-1/4}$ with $b_\mu=0.052$, $b_\pi=0.054$, and $b_p=0.059$. Fig. 2 shows a comparison of directly calculated $\langle\theta_2^2\rangle^{1/2}$ with rms angles from the parametrization.

Nuclear recoil is a negligible source of energy loss even though it is highly localized. For a light nucleus such as aluminum the kinetic energy of recoil in a typical bremsstrahlung event is in the 1-50 KeV region for incident particles in the TeV regime. Recoils in excess of 1 MeV occur only when v is very near unity. For heavy nuclei there is even less recoil energy. Therefore <u>nuclear</u> recoil can generally be neglected in energy deposition calculations. The photon energy then follows from energy conservation. The rms angle of the photon is fitted by:

$$\langle\theta_\gamma^2\rangle^{1/2} = [a_i+b_i(-\ln v)^d]E^{-c} \qquad (7)$$

with a_μ=0.127, a_π=0.157, a_p=0.940, b_μ=0.058, b_π=0.072, b_p=0.126, $c=0.94+0.06v^3$, $d_\mu=d_\pi=1/2$, $d_p=1$. The fits are illustrated in fig. 3. Again a slight Z dependence is ignored.

As already mentioned the bremsstrahlung contributions off atomic electrons are added incoherently and are separately parametrized. For photon emission by the incident particle, the v-distribution obeys:

$$\begin{aligned} \sigma^{-1}d\sigma/dv &= k_1 v^{-0.95} && v_{min} < v < 0.05 \\ &= k_2 v^{-n} && 0.05 < v < v_2 \\ &= k_3(v_{max}-v)^{1/2} && v_2 < v < v_{max} \end{aligned} \qquad (8).$$

where $n_\mu=n_\pi=1.50-0.030\ln E$, $n_p=1.45$ and $v_2=v_{2,coh}\cdot v_{max}$, where $v_{2,coh}$ is the v_2 for the coherent nuclear case and v_{max} is the maximum kinematically allowed v. Under the condition $m_i \gg m_e$, $v_{max}=2m_eE/(2m_eE+m_i^2)$, where m_i is the mass of the incident particle. The k_i are again fixed by continuity and normalization. The fit is shown in fig. 4 for a few cases.

The scattering angle of the incident μ or π may be represented by:

$$\begin{aligned} \langle\theta_2^2\rangle^{1/2} &= 0.016(v/E)^{1/2} && v < 0.003 \\ &= k_1 v^n && 0.003 < v < 0.3 \\ &= k_2(1-v)^{-0.81} && 0.3 < v < v_{max} \end{aligned} \qquad (9)$$

where $n=0.84-0.060\ln E$. For incident p:

$$\langle\theta_2^2\rangle^{1/2} = 0.019(v/E)^{1/2} \qquad v < 0.3$$
$$= k_2(1-v)^{-0.96} \qquad 0.3 < v < v_{max} \qquad (10).$$

The k_i are fixed by continuity. Calculated results are compared with the parametrization in fig. 5.

Because of its light mass the kinetic energy of the recoiling electron is typically not negligible. The average kinetic energy of recoil, $\langle T_R\rangle$, as a function of v is approximately:

$$\langle T_R\rangle = [a_i v/(b_i+v)]\cdot\exp[c_i v^n(1-v_{max})^2/(1-v)^2] \qquad (11)$$

where $a_\pi=35E^{0.15}$, $a_p=15E^{0.55}$, $b_\pi=100E^{-0.85}$, $b_p=40E^{-0.45}$, $c_\pi=4$, $c_p=2$, $n_\pi=4$, $n_p=1$. This is illustrated in fig. 6. Since this is never a dominant process it appears sufficient to assign the value $\langle T_R\rangle$ to each electron recoil rather than sample from a distribution about $\langle T_R\rangle$.

The energy of the γ follows form energy conservation. Its rms angle is fitted by:

$$\langle\theta_\gamma^2\rangle^{1/2} = [5.7\cdot10^{-3}E^{-2}v^{-1},\ b_iE^{-3/2}(1-v)^{-1/2}]_{max} \qquad (12)$$

with $b_\pi=0.41$ and $b_p=2.7$. Some fits are shown in fig. 7. The angle of the recoiling electron may be obtained by momentum conservation. In the peaking approximation the event is co-planar and the γ and the scattered particle appear on the same side.

For bremsstrahlung by the recoiling electron the v-distribution of the incident particle follows:

$$\sigma^{-1}d\sigma/dv = k(1-v)^{1/2}v^{-1}(v+5v_o)^{-1} \qquad (13)$$

where k is a normalization constant and v_o=0.001/E. The quality of the fit is shown in fig. 8.

The angle of the scattered particle is fitted by:

$$\langle\theta_2^2\rangle^{1/2} = [0.028(E(1-v)/v)^{-1/2},\ 5\cdot10^{-4}/m_i]_{min} \qquad (14)$$

where m_i is the mass of the incident particle. This is illustrated in fig. 9. For this process the recoil electron carries the major share of the energy lost by the incident particle. To good approximation:

$$\langle T_R\rangle = 0.93Ev \qquad (15).$$

The rms angle of the electron, as shown in fig. 10, is well represented by:

$$\langle\theta_R^2\rangle^{1/2} = 0.033(Ev)^{-1/2}(1-v)^n \qquad (16)$$

where $n=a_i+b_i/\ln E$ with a_π=-0.15, a_p=-1.55, b_π=3.5, b_p=20. The energy and angle of the γ follow from energy and momentum conservation similar to process (iii), above.

4. Direct Pair Production

4.1. Calculation

The basic differential cross section for pair production by charged particles is derived by Kel'ner [14]. It applies to the case of a stationary (infinitely heavy) nucleus but where all other particles are relativistic. The lowest order

diagrams are integrated analytically and a closed form expression is obtained (up to screening corrections) for $d\sigma/dtd\epsilon_+d\epsilon_-$, where t is the four momentum transfer to the incident particle and the $\epsilon_\pm$ are the energies of the pair members. This derivation does not include a nuclear form factor. The difficulties with this are mentioned by Kel'ner but these are readily overcome with some numerical effort. The relevant integrals of Kel'ner are evaluated analytically to yield an expression for $d\sigma/dtd\epsilon_+d\epsilon_-dq^2$ where q^2 is the momentum transfer to the nucleus. A nuclear form factor e.g., of the dipole type as in the bremsstrahlung calculations can then be inserted and the remaining integrations performed numerically. Screening is likewise introduced at this level by the Thomas-Fermi-Moliere atomic form factor [9]. A check is provided by performing the same integrations without form factors and comparing with Kel'ner's analytical results. The introduction of these form factors is limited to the dominant diagrams (those with a virtual electron). The virtual muon diagrams contribute only about 0.1% to dE/dx and are significant only for production of very energetic pairs near the kinematic limit [15]. These are added unaltered from Kel'ner's derivation.

For studies of the detailed spatial distribution of energy deposition some information on the produced pair is needed. From the selection of outgoing energy and angle the four momentum transfer to the incident particle, $k_1=(\omega,\vec{k}_1)$, is determined. The angle, α, between $\vec{k}_1$ and the total momentum of the pair, $\vec{p}_\pm$, can be calculated in an approximate way provided the averages $\langle -q^2\rangle$ and $\langle qk_1\rangle$ as a function of v are known. Since $\vec{p}_\pm = \vec{p}_+ + \vec{p}_- = \vec{k}_1 + \vec{q}$ it follows that:

$$\begin{aligned}\cos\alpha &= \vec{p}_\pm \cdot \vec{k}_1 / |\vec{p}_\pm| \cdot |\vec{k}_1| \\ &= (\omega^2 - k_1^2 - qk_1)/[(\omega^2 - M^2)(\omega^2 - k_1^2)]^{1/2} \end{aligned} \qquad (17)$$

with $M=(q^2+2qk_1+k_1^2)^{1/2}$ being the invariant mass of the pair. Using the small angle approximation eq. (17) reduces to:

$$\alpha^2 = [-q^2-(-q^2)_{min}]/|\vec{p}_\pm|^2 \qquad (18)$$

where $|\vec{p}_\pm|^2=\omega^2-k_1^2-2qk_1-q^2$ and $(-q^2)_{min}=(qk_1)^2/(\omega^2-k_1^2)$.

A reasonable MC algorithm consist of selecting $Q^2=-q^2-(-q^2)_{min}$ from a one sided Gaussian with zero mean and $\sigma^2=-\langle q^2\rangle-\langle(qk_1)^2\rangle/(\omega^2-k_1^2)$. If, in the definition of $(-q^2)_{min}$, $(qk_1)^2$ is replaced by $-q^2\langle(qk_1)^2\rangle/\langle q^2\rangle$ then

$$-q^2 = Q^2/[1-\langle(qk_1)^2\rangle/\langle q^2\rangle(\omega^2-k_1^2)] \qquad (19).$$

The angle α is then obtained form eq. (18) by similarly replacing qk_1 in the expression for $|\vec{p}_\pm|$ in the denominator:

$$\alpha^2 = -q^2\cdot[1+\langle(qk_1)^2\rangle/\langle-q^2\rangle(\omega^2-k_1^2)] \\ /[\omega^2-k_1^2-2\langle qk_1\rangle(-q^2/\langle-q^2\rangle)^{1/2}-q^2] \qquad (20).$$

The azimuthal angle of $\vec{p}_\pm$ about the direction of the incident particle is chosen uniformly. The opening angle of the pair, β, is related to M^2 and to $x_+(\equiv\epsilon_+/\omega)$. Since the cross section depends rather weakly on x_+, a uniform distribution $(m_e/\omega\leq x_+ \leq 1-m_e/\omega)$ is assumed. From $M^2=2(m_e^2+\epsilon_+\epsilon_--|\vec{p}_+\vec{p}_-|\cos\beta)$ and from treating the pair members relativistically it follows that:

$$\beta^2 \simeq M^2/x_+x_-\omega^2 \qquad (21)$$

and therefore

$$\beta^2 = [q^2+2\langle qk_1\rangle(-q^2/\langle-q^2\rangle)^{1/2}+k_1^2]/x_+(1-x_+)\omega^2 \qquad (22)$$

where again $\langle qk_1\rangle(-q^2/\langle-q^2\rangle)^{1/2}$ replaces qk_1 and the azimuthal opening angle is again uniformly distributed.

Electron targets are treated similar to nuclei except that an inelastic form factor replaces the nuclear form factor and no screening is present. In addition some information on target recoil is needed which in the nuclear case is neglected. The average kinetic energy of recoil, $\langle T_R \rangle$, is related to $\langle -q^2 \rangle$:

$$\langle T_R \rangle = \langle -q^2 \rangle / 2m_e \qquad (23)$$

and $\langle -q^2 \rangle$ is a known function of v. Similarly to bremsstrahlung off electrons, each recoil is assumed to have a fixed kinetic energy $\langle T_R \rangle$. (To conserve energy an amount $\langle T_R \rangle$ must be deducted from the energy of the other outgoing particles.)

For the purpose of determining the recoil angle it is assumed that the cross section as written by Kel'ner applies to a collision in a Breit frame of reference where the condition of arbitrary momentum transfer and zero energy transfer is explicitly realized. The angle between recoiling electron and incident particle is then transformed to the lab. The average lab angle shows very little variation with v and is approximately equal to $\pi/4$. A reasonable algorithm may be to sample from a distribution uniform in angle from 0 to $\pi/2$.

In principle, electron target recoil should also be included in the analysis of the produced pair. However the underlying assumption $\omega >> T_R$ still hold reasonably well over most of the range of v (except where v is small in which case a more accurate algorithm gains very little). This justifies using the same simulation for pair production off electron targets as off nuclear ones.

4.2. Results

The v-distribution for direct pair production off both nuclear and electron targets is well approximated by:

$$\begin{aligned}
\sigma^{-1}d\sigma/dv &= k_o && 5m_e/E < v < 25m_e/E \\
&= k_1 v^{-1} && 25m_e/E < v < v_{1,i} \\
&= k_2 v^{-2} && v_{1,i} < v < v_{2,i} \\
&= k_3 v^{-3} && v_{2,i} < v < 1
\end{aligned} \qquad (24)$$

where $v_{1,\mu}=v_{1,\pi}=2\cdot10^{-3}$, $v_{1,p}=10^{-4}$, $v_{2,\mu}=v_{2,\pi}=2\cdot10^{-2}$ and $v_{2,p}=5\cdot10^{-3}$. The k_i follow once again from continuity and normalization. If $25m_e/E$ is larger than $v_{1,i}$ the segment with the v^{-1} dependence is omitted. If $25m_e/E$ is larger than $v_{2,i}$ the v^{-2} segment is also omitted. The dependence of $\sigma^{-1}d\sigma/dv$ on Z is rather weak and is neglected.

For very small v Kel'ner suggests using

$$d\sigma/dv \propto v^{-1}\sigma_o(Ev)\ln(m_e/v) \qquad (25)$$

in lieu of the general expression, where $\sigma_o(w)$ is the total cross section for pair production by a photon of energy w. Ignoring the log factor, $d\sigma/dv$ follows a v^{-1} dependence in the region where $\sigma_o=\sigma_o(\infty)$ is constant (w>1 MeV). This is also true in eq. (24). Below $w\simeq5m_e$, σ_o remains small [$<0.05\sigma_o(\infty)$] whereupon it climbs roughly linearly until $w\simeq25m_e$ [where $\sigma_o\simeq\sigma_o(\infty)/2$]. These considerations lead to the low v part of eq. (24). Fig. 11 compares the approximation with direct computation.

The lab angle of the outgoing particle following pair production is parametrized as:

$$\begin{aligned}
\langle\theta_2^2\rangle^{1/2} = {} & (2.3+\ln E)E^{-1}(1-v)^n(v-2m_e/E)^2v^{-2} \\
& \cdot[a_i v^{1/4}(1+b_i E)+c_i v/(v+d_i),\ e_i]_{min}
\end{aligned} \qquad (26)$$

where n depends on particle type with $n_\mu=n_\pi=-1$, $n_p=-0.1\ln E$, $a_\mu=8.9\cdot10^{-4}$, $a_\pi=9.2\cdot10^{-4}$, $a_p=1.06\cdot10^{-3}$, $b_\mu=b_\pi=1.5\cdot10^{-5}$, $b_p=0.$, $c_\mu=0.032$, $c_\pi=0.053$, $c_p=0.090$, $d_\mu=1.0$, $d_\pi=1.3$, $d_p=0.35$, $e_\mu=0.10$, $e_\pi=0.12$, $e_p=\infty$. Again a slight Z dependence of $\langle\theta_2^2\rangle^{1/2}$ is ignored. Comparisons between directly calculated $\langle\theta_2^2\rangle^{1/2}$ and eq. (26) are shown in fig. 12.

The average of the square of the momentum transfer to the nucleus is approximated by:

$$\begin{aligned}\langle -q^2\rangle &= [6.0\cdot10^{-6}(\mathrm{Ev})^{1/4},\ 3.3\cdot10^{-6}]_{\min} \\ &\quad +(a_i+b_iZ^{-1/2})\cdot(v/v_o)^{\alpha} && v < v_{1,i} \\ &= (c_i+d_iE^{-m})Z^{-1/2} && v_{1,i} < v < 1 \end{aligned} \qquad (27)$$

where $v_{o,\pi}=3\cdot10^{-3}$, $v_{o,p}=8\cdot10^{-4}$, $v_{1,\pi}=0.20+0.20Z^{-1/2}$, $v_{1,p}=0.085+0.13Z^{-1/2}$, $a_\pi=1.9\cdot10^{-6}$, $a_p=4.0\cdot10^{-6}$, $b_\pi=5.6\cdot10^{-6}$, $b_p=9.5\cdot10^{-6}$, $c_\pi=6.3\cdot10^{-4}$, $c_p=0$, $d_\pi=4.8\cdot10^{-3}$, $d_p=2.7\cdot10^{-2}$, $m_\pi=1/3$, $m_p=1/4$. The exponent α depends also on particle type and is derived from continuity at $v_{1,i}$. Some results are shown in fig. 13. The relatively strong Z dependence for larger v is a consequence of the introduction of a nuclear form factor.

The average value of the product of the four momentum transfers to the target and to the incident particle is represented as:

$$\begin{aligned}\langle -qk_1\rangle &= (av^n+b_iv^{1.64})E^{0.3} && v < 0.5 \\ &= c && v \geq 0.5 \end{aligned} \qquad (28)$$

where $n=0.3(6.45+\ln E)/(1.72+\ln E)$, $a=8.11\cdot10^{-6}/(5.6\cdot10^{-3})^n$, $b_\pi=0.04$, $b_p=0.53$, and c follows from continuity. The Z dependence is much weaker than for $\langle -q^2\rangle$ and is neglected. The fits are illustrated in fig. 14.

5. Nuclear Interaction of Muons

5.1. Calculation

The differential cross section used for inelastic scattering of muons is the usual lepto-production scaling formula [16] with experimentally measured structure functions. The parametrization of the scaling function, νW_2, for protons is from Bodek et al. [17] with corrections in the low invariant mass region from Breidenbach and Kuti [18]. For $|q^2| < 0.15$ GeV^2, $\nu W_2 = |q^2|$ is adopted [19] (q^2 in GeV^2) with the same corrections in the resonance region. For neutrons $\nu W_2^n = \nu W_2^p(1-0.75x)$ is assumed [20] where x is the Bjorken scaling variable. W_1 is related to W_2 via $W_1 = W_2(1+\nu^2/|q^2|)/\nu(1+R)$ where ν is the total energy carried by hadrons and R=0.18 is assumed everywhere. Nuclear targets are considered a simple superposition of protons and neutrons. Fermi motion, shadowing, EMC effect, etc. are not included.

The cross section given by the lepto-production scaling formula refers to inelastic scattering unaccompanied by photon emission. The parametrizations used are from data which correct for this effect. To account for such events these radiative corrections must be undone either by re-introducing them into the cross section or, what seems preferable, to insert them directly into the MC simulation. The method of equivalent radiators [21] is particularly easy to apply: the internal bremsstrahlung is approximated by the radiation emitted due to two radiators of thickness $L=(\alpha/\pi)[\log(-q^2/m^2)-1]$, where α is the fine structure constant, placed before and after the scattering event. The scattering in these radiators is treated as ordinary external bremsstrahlung.

5.2. Results

The only two quantities of interest here are $\sigma^{-1}d\sigma/dv$ and $\langle\theta_2^2\rangle^{1/2}$. Since the internal bremsstrahlung is treated separately in the MC, the formulae and graphs of these two quantities appearing in this section pertain to bare scattering. However, the graphs of $\langle\theta_2^2\rangle^{1/2}$ and dE/dx in bulk matter in the final section include the internal bremsstrahlung.

The fractional energy loss distribution is well represented by:

$$\sigma^{-1}d\sigma/dv = k_1(Ev)^2 \qquad 0.144 < Ev < 0.35$$

$$= k_2(Ev)^{-1.11}(1-v)^2 \qquad 0.35 < Ev < E-m \qquad (29).$$

The lower limit of 0.144 GeV is the kinematical limit ($\simeq m_o+m_o^2/2m_N$) for producing a single π^o (mass=m_o). Comparison of eq. (29) with direct calculation from the basic formula is shown in fig. 15.

The rms angle of the scattered μ is represented by:

$$\langle\theta_2^2\rangle^{1/2} = [0.39/E(1-v)]\,[E^{1/2}v(1-v)]^{0.17}(1-0.135/Ev) \qquad (30).$$

The quality of the fit is illustrated in fig. 16.

The basic results for both $\sigma^{-1}d\sigma/dv$ and $\langle\theta_2^2\rangle^{1/2}$ show a certain amount of structure in the region Ev $\simeq$ 1 GeV owing to the parametrization of Breidenbach and Kuti which represents resonance formation at low invariant mass. For most applications this structure may be replaced by a smooth approximation as is done in eqs. (29) and (30). If need be the structure could be restored upon multiplication by a tabulated function which is unity outside the resonance region.

6. RMS Angle and Energy Loss in Bulk Matter Comparison with Other Work

By averaging $\langle\theta_2^2\rangle$, obtained as a function of v for each process, over all v and multiplying by the average number of events per unit length an average deflection per unit length, $\langle\overline{\theta_2^2}\rangle$, is obtained. Since (small) angles combine by summing their squares $\langle\overline{\theta_2^2}\rangle$ has the virtue of being proportional to target length. However, it appears more suitable to present results for $\langle\overline{\theta_2^2}\rangle^{1/2}$. Note that for the processes discussed here $\langle\overline{\theta_2^2}\rangle^{1/2}$ is strictly a thin target concept since, even without any other type of interactions, a particle may lose a considerable amount of energy in producing a γ or e^* pair. This lower energy particle is now characterized by a larger $\langle\overline{\theta_2^2}\rangle^{1/2}$ and $\langle\overline{\theta_2^2}\rangle$ resulting from summing over multiple events is no longer proportional to target thickness. This is to be contrasted with e.g., rms angles for multiple Coulomb scattering.

In spite of their limited usefulness it is nonetheless of interest to compare the $\langle\overline{\theta_2^2}\rangle^{1/2}$ for the various processes among themselves and with rms angles for multiple Coulomb scattering. Figs. 17 and 18 present $\langle\overline{\theta_2^2}\rangle^{1/2}$ for muons and protons on beryllium, soil (Z=11, A=23), iron and lead. The rms angles for multiple Coulomb scattering are from a standard expression [22]. The rms angles for pair production off nuclear targets and atomic electrons are combined. The plots show also the $\langle\overline{\theta_2^2}\rangle^{1/2}$ for incoherent (quasi-elastic) bremsstrahlung. It is seen to be comparable to pair production $\langle\overline{\theta_2^2}\rangle^{1/2}$ for light nuclei and that both are relatively small.

Fig. 17 also shows some calculated results of Alsmiller et al. [23] in the $E \leq 500$ GeV region. There is acceptable agreement for bremsstrahlung and pair production but obvious discrepancies exist for $\langle\theta_2^2\rangle^{1/2}$ from nuclear interactions. Without a detailed investigation it appears that the origin of the larger $\langle\theta_2^2\rangle^{1/2}$ of Alsmiller et al. is that in the integration over $\nu(\equiv E-E')$ their lower limit is (essentially) zero [24]. But this includes an unphysical region where ν is less than the kinematical limit ($\sim m_\pi$).

Figs. 19 and 20 present the average stopping powers, obtained in the course of calculating the rms angles, for muons and protons in soil and iron. Again pair production off nuclei and electrons is combined. For comparison dE/dx due to collision losses [25] is also displayed. The elastic radiative correction is applied to dE/dx from collision losses and is approximated by:

$$\Delta(dE/dx) = \int_0^{|T|} \delta \cdot (d\sigma/dt)_{el} \cdot (|t|/2m_e) \cdot F \cdot d|t| \qquad (31)$$

where $|T|$ is the maximum momentum transfer, δ is the elastic radiative correction to elastic projectile-electon scattering, $|t|/2m_e$ is the kinetic energy of the recoiling electron, F is the inelastic atomic form factor and $(d\sigma/dt)_{el}$ represents the Rosenbluth formula with appropriate form factors. The standard Bethe-Bloch formula assumes essentially that both the electric and magnetic form factors are unity (which holds for muons but not for hadrons). A second correction to the standard dE/dx for hadrons may therefore be evaluated:

$$\Delta(dE/dx) = \int_0^{|T|} [(d\sigma/dt)_R - (d\sigma/dt)_M] \cdot (|t|/2m_e) \cdot F \cdot d|t| \qquad (32)$$

where $(d\sigma/dt)_{R,M}$ denote the Rosenbluth and Mott scattering cross sections, respectively. The result after both corrections (when applicable) are made is shown by the dotted line in figs. 19 and 20.

Fig. 19 compares also the results of Theriot [26] in the $E \leq 500$ GeV region. Agreement for bremsstrahlung and pair production is good although the latter appear to be diverging with increasing energy. Results for nuclear interaction disagree by a factor of ~2. Fig. 19(b) also shows the recent results of Lohmann et al. [27] which show closer agreement.

The elastic radiative correction to dE/dx and the bremsstrahlung contribution from recoiling electrons are compared on a more suitable scale in fig. 21 for muons in soil. Above about 100 GeV the electron bremsstrahlung is clearly larger. Also pictured is the inelastic part of the radiative correction pertaining only to target radiation. This is also evaluated using eq. (31) but with a different δ (see refs. 7 and 12) and with a correction added to the kinetic energy of recoil to represent the photon energy. This is a roughly equivalent way to calculate the electron bremsstrahlung if the parameter ΔE in the expression for δ is interpreted as the maximum energy carried off by the photon. This is taken to be of the order of the kinetic energy of recoil. The results depend logarithmically on ΔE and are shown in fig. 21 for $\Delta E = T_R/2$, T_R and $2T_R$. The calculation in the projectile restframe should be the more accurate one but the radiative correction result serves well to confirm the observed trend.

Fig. 22 compares the bremsstrahlung contribution of the electron recoil to dE/dx with both elastic and inelastic radiative corrections and with the correction arising from inclusion of the form factors [eq. (32)] for the case of protons in

soil. It is seen that the latter becomes substantial around 1 TeV. (For pions this occurs at even lower energies.) This means that at these energies a significant fraction of events proceed via inelastic channels. The average energy loss accompanying these events is much larger than indicated by eq. (32) or fig. 22 since this assumes elastic scattering while the energy loss in inelastic events is inevitably much larger. The systematics of inelastic energy losses is being further investigated [8].

My thanks to J.D. Bjorken for an enlightening discussion on the subject of radiative corrections, and to D.A. Edwards and F. Turkot for their helpful criticism of the manuscript.

References

[1] Reference Design Study for the SSC, Reference Design Study Group, Berkeley (1984).

[2] A. Van Ginneken, Fermilab FN-272 (1975).

[3] R.J. Glauber, Lectures in Theoretical Physics, W.E. Brittin et al., Eds., Vol.I, Interscience Publ., New York, (1959), p 315ff; R.J. Glauber and G. Matthiae, Nucl. Phys. B21 (1970) 133.

[4] L. Landau and I. Pomeranchuk, Doklady Akad. Nauk. S.S.S.R. 92 (1953) 535 ; A.B. Migdal, Phys. Rev. 103 (1956) 1811.

[5] H. Messel and D.F. Crawford, Electron-Photon Shower Distribution Functions, Pergamon Press, Oxford (1970).

[6] see e.g., J.D. Jackson, Classical Electrodynamics, 2nd Ed., Wiley, New York (1975), p. 674ff.

[7] L.W. Mo and Y.S. Tsai, Rev. Mod. Phys. 41 (1969) 205.

[8] S. Qian and A. Van Ginneken, in preparation.

[9] Y.S Tsai, Rev. Mod. Phys. 46 (1974) 815.

[10] see e.g., H.W. Koch and J.W. Motz, Rev. Mod. Phys. 31 (1959) 920.

[11] R.R. Wilson, in Proc. 1971 Int. Symp. on Photon and Electron Interactions at High Energies, Cornell Univ. Ithaca, N.Y. (1972).

[12] Y.S. Tsai, Phys.Rev. 122 (1961) 1898 ; see also N.T. Meister and D.R. Yennie, Phys. Rev. 130 (1975) 1210.

[13] R.R. Roy and R.D. Reed, Interactions of Photons and Electrons with Matter, Academic Press, New York (1968); see also ref. 10.

[14] S.R. Kel'ner, Sov. J. Nucl. Phys. 5 (1967) 778.

[15] S.R. Kel'ner and Yu.D. Kotov, Sov. J. Nucl. Phys. 7, (1968) 237.

[16] J.D. Bjorken, Phys. Rev. 163 (1967) 1767.

[17] A. Bodek et al., Phys. Rev. D20 (1979) 1471.

[18] M. Breidenbach and J. Kuti, Phys. Lett., 41B (1972) 345.

[19] This is close to the parametrization of W. Constandt et al., 16th Int. Cosmic Ray Conf., Vol. 10, Kyoto, Japan (1979), p. 233ff.

[20] see e.g., F.E. Close, An Introduction to Quarks and Partons, Academic Press, New York (1979).

[21] J.D. Bjorken, Ann. Phys. (N.Y.) 24 (1963) 201.

[22] see e.g., M.Aguilar-Benitez et al., Rev. Mod. Phys. 56 (1984) S113. The multiple scattering formula is used in the thin target approximation.

[23] R.G. Alsmiller,Jr., et al., ORNL TM-3356 (1971).

[24] The treatment of Alsmiller et al. is based on K. Kobayakawa, Nuovo Cim. 47 (1967) 156.

[25] see e.g., U. Fano, Ann. Rev. Nucl. Sci. 13 (1963) 1.

[26] D. Theriot, Fermilab TM 229 (1970).

[27] W. Lohmann et al., CERN 85-03 (1985).

Figure Captions

Fig. 1. (a) Probability for γ emission ($E_\gamma \geq 1$ MeV) off nuclear targets as a function of v, E_γ as a fraction of the incident energy. In figs. 1-16 the symbols represent direct calculation (in this case using the Mo-Tsai formula) and the curves are the empirical fits. Here only a v^{-1} line is drawn near the symbols to avoid clutter. The values for incoherent bremsstrahlung are normalized to the total coherent cross section for comparison.

(b) Same as fig. 1 (a) but for $v \geq 0.1$. Curves here represent the fits from eq. (5).

Fig. 2. (a) Rms angle of scattered particle undergoing nuclear bremsstrahlung as a function of v, in small v region.

(b) as in (a) but for $v \geq 0.5$, as a function of (1-v).

Fig. 3. Rms angle of (nuclear) bremsstrahlung γ with respect to incident direction as a function of v.

Fig. 4. (a) Probability for γ emission ($E_\gamma \geq 1$ MeV) by incident particle off atomic electron target as a function of v in the small v region. Here only a $v^{-0.95}$ line is drawn near the points to avoid clutter.

(b) as in (a) but for $v \geq 0.1$. Here the curves are fits from eq. (8).

Fig. 5. Rms angle of particle undergoing bremsstrahlung off atomic electron as a function of v.

Fig. 6. Kinetic energy of recoil of electron (for the process where the incident particle emits the γ) as a function of v.

Fig. 7. Rms angle of γ emitted by incident particle off atomic electron as a function of v.

Fig. 8. Probability for γ emission ($E_\gamma \geq 1$ MeV) by atomic electron off incident particle as a function of v.

Fig. 9. Rms angle of scattered particle (for the process where the electron emits a γ) as a function of v.

Fig. 10. Rms angle of recoil of electron following bremsstrahlung by the electron as a function of v.

Fig. 11. Probability of emission of e^* as a function of v, the total pair energy expressed as a fraction of the incident energy.

Fig. 12. Rms angle of scattered particle following direct pair production off a nuclear target as a function of v.

Fig. 13. Average value of the square of the momentum transfer to nuclear target as a function of v.

Fig. 14. Average value of the product of the four momentum transfer to the nucleus and the four momentum transfer to the incident particle as a function of v.

Fig. 15. Probability of muon deep inelastic scattering as a function of v, the total hadronic energy in the lab expressed as a fraction of the incident energy.

Fig. 16. Rms angle of the muon following deep inelastic scattering as a function of v.

Fig. 17. Rms angle in bulk matter for muons as a function of energy due to the various processes in (a) beryllium, (b) soil, (c) iron and (d) lead. Also shown are comparisons with Alsmiller

et al. in (b) and (c). Legend: BS, bremsstrahlung; (coh), coherent (inc), incoherent nuclear; (eμ), muon vertex (ee), electron vertex, atomic electron; DIS, deep inelastic scattering; pp, pair production; mCs, multiple Coulomb scattering.

Fig. 18. Rms angle in bulk matter for protons as a function of energy due to the various processes in (a) beryllium, (b) soil, (c) iron and (d) lead. Legend: see fig. 17.

Fig. 19. Muon stopping power as a function of energy due to the various processes in (a) soil and (b) iron. Also shown are comparisons with the work of Theriot and Lohmann et al. Legend: CL, collision energy losses; others, see fig. 17.

Fig. 20. Proton stopping power as a function of energy due to the various processes in (a) soil and (b) iron. Legend: see figs. 17 and 19.

Fig. 21. Contributions and corrections to muon stopping power in soil as a function of energy. Solid lines are the inelastic radiative correction evaluated for various ΔE. Dashed line is the elastic radiative correction. Dot-dash line is the bremsstrahlung contribution by atomic electrons off the muon projectile. Legend: RC, radiative correction; others, see figs. 17 and 19.

Fig. 22. Contributions and corrections to proton stopping power in soil as a function of energy. Solid line is the inelastic radiative correction evaluated for $\Delta E=T_R$, the kinetic energy of recoil. Dashed line is the elastic radiative correction. Dot-dash line is the bremsstrahlung contribution by atomic electrons off the proton projectile. Legend: FF cor, correction due to the presence of form factors ($\neq 1$) in elastic scattering cross section; others, see figs. 17, 19 and 21.

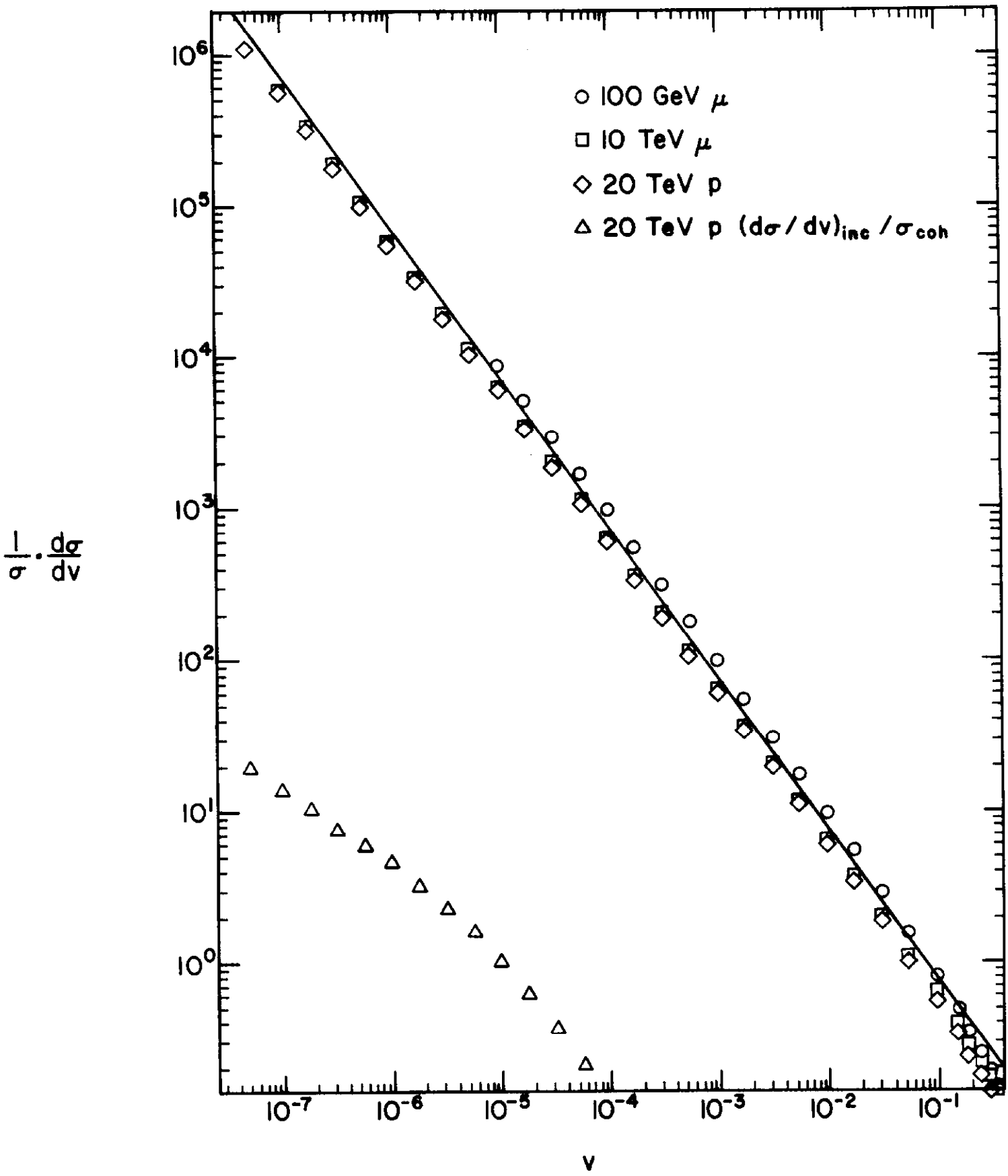
○ 100 GeV μ
□ 10 TeV μ
◇ 20 TeV p
△ 20 TeV p (dσ/dv)inc /σcoh
10^6
10^5
10^4
10^3
10^2
10^1
10^0
10^-7
10^-6
10^-5
10^-4
10^-3
10^-2
10^-1
v
1/σ · dσ/dv

Fig. 1.a

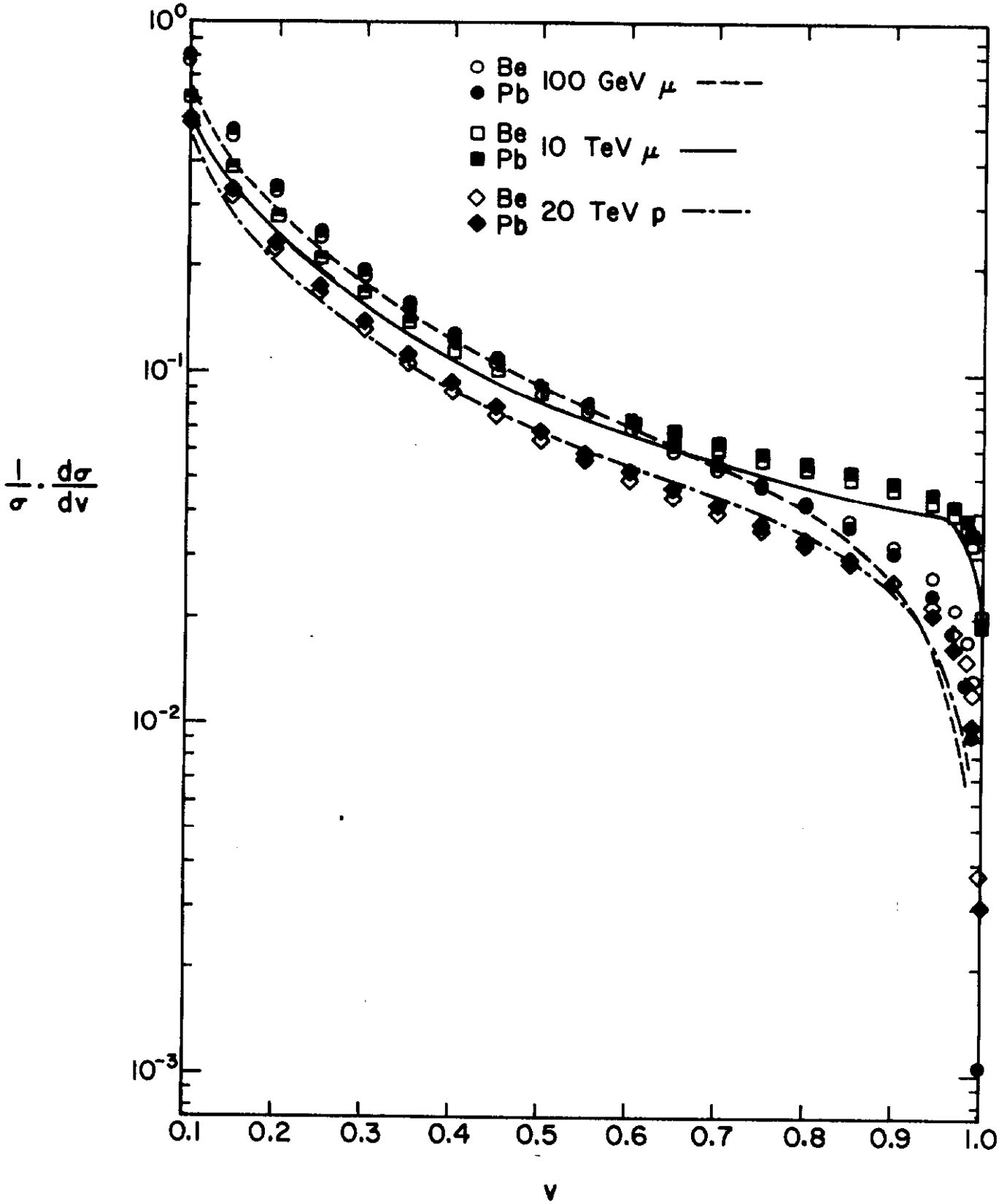
10^0
10^-1
10^-2
10^-3
0.1
0.2
0.3
0.4
0.5
0.6
0.7
0.8
0.9
1.0
ν
1/σ · dσ/dν
Be
Pb
100 GeV μ
Be
Pb
10 TeV μ
Be
Pb
20 TeV p

Fig. 1.b

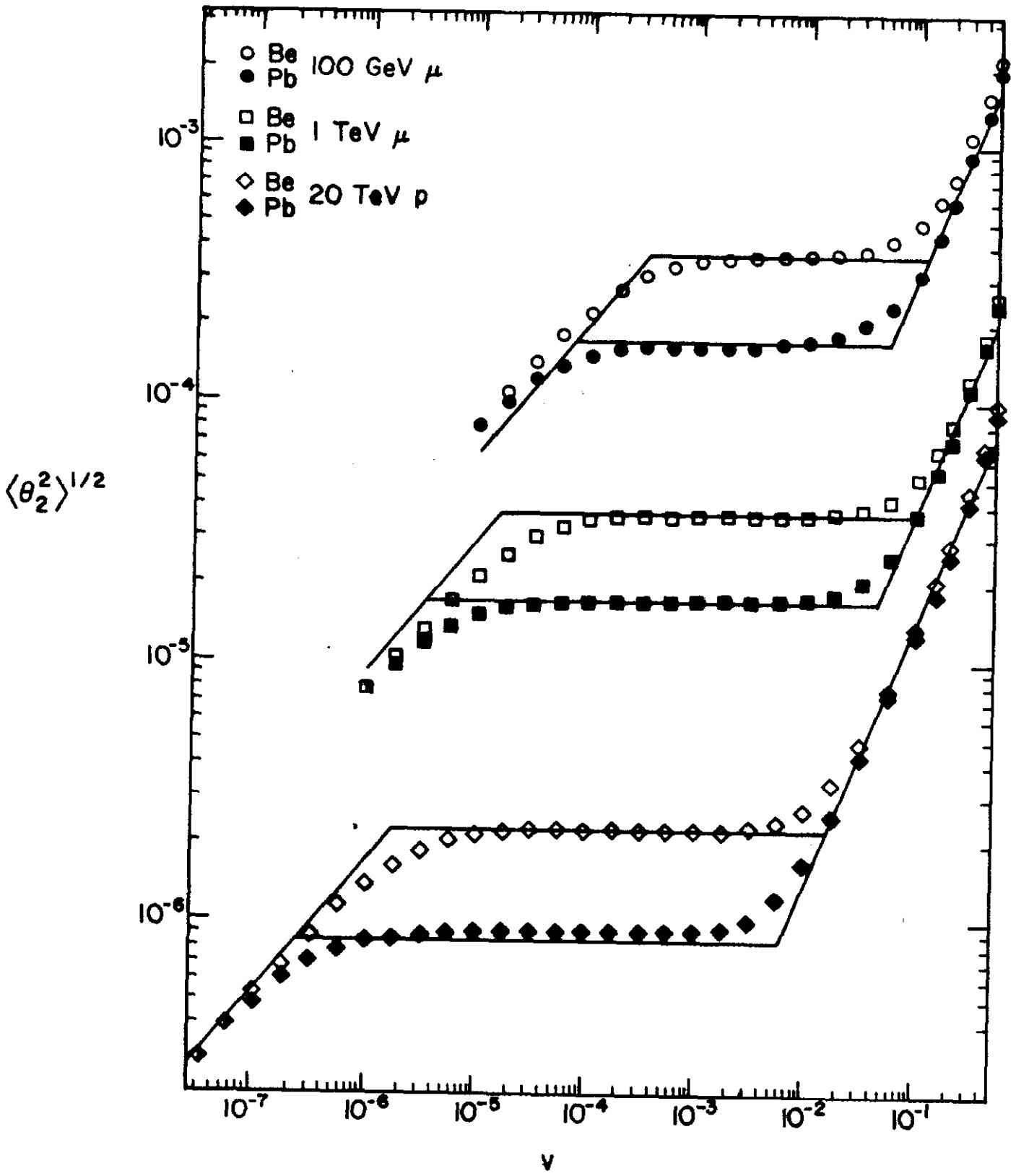
Be
Pb
100 GeV μ
Be
Pb
1 TeV μ
Be
Pb
20 TeV p
$\langle\theta_2^2\rangle^{1/2}$
10^{-3}
10^{-4}
10^{-5}
10^{-6}
10^{-7}
10^{-6}
10^{-5}
10^{-4}
10^{-3}
10^{-2}
10^{-1}
ν

Fig. 2.a

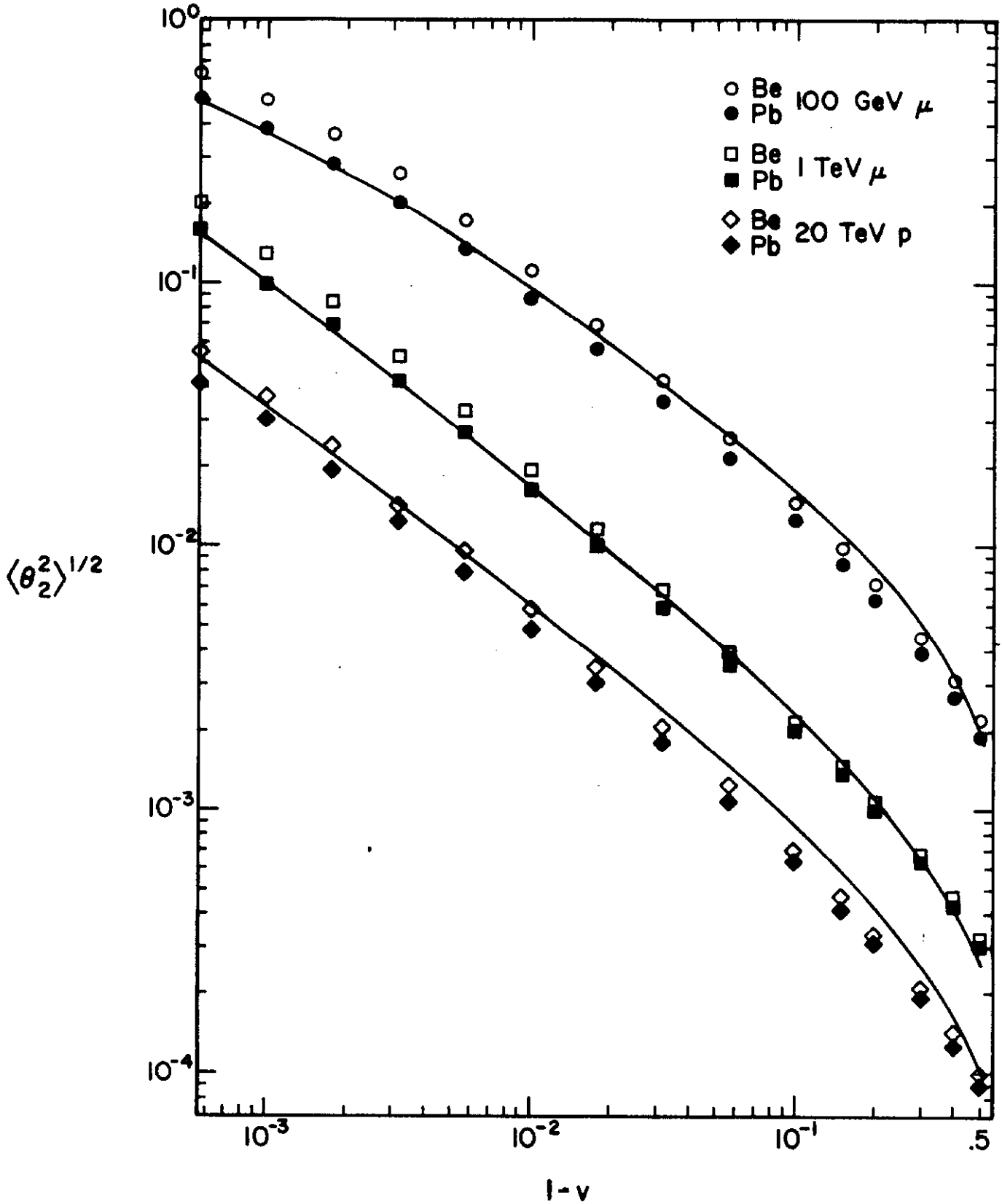
10^0
10^{-1}
10^{-2}
10^{-3}
10^{-4}
$\langle\theta_2^2\rangle^{1/2}$
Be
Pb
100 GeV μ
Be
Pb
1 TeV μ
Be
Pb
20 TeV p
10^{-3}
10^{-2}
10^{-1}
.5
1 - v

Fig. 2.b

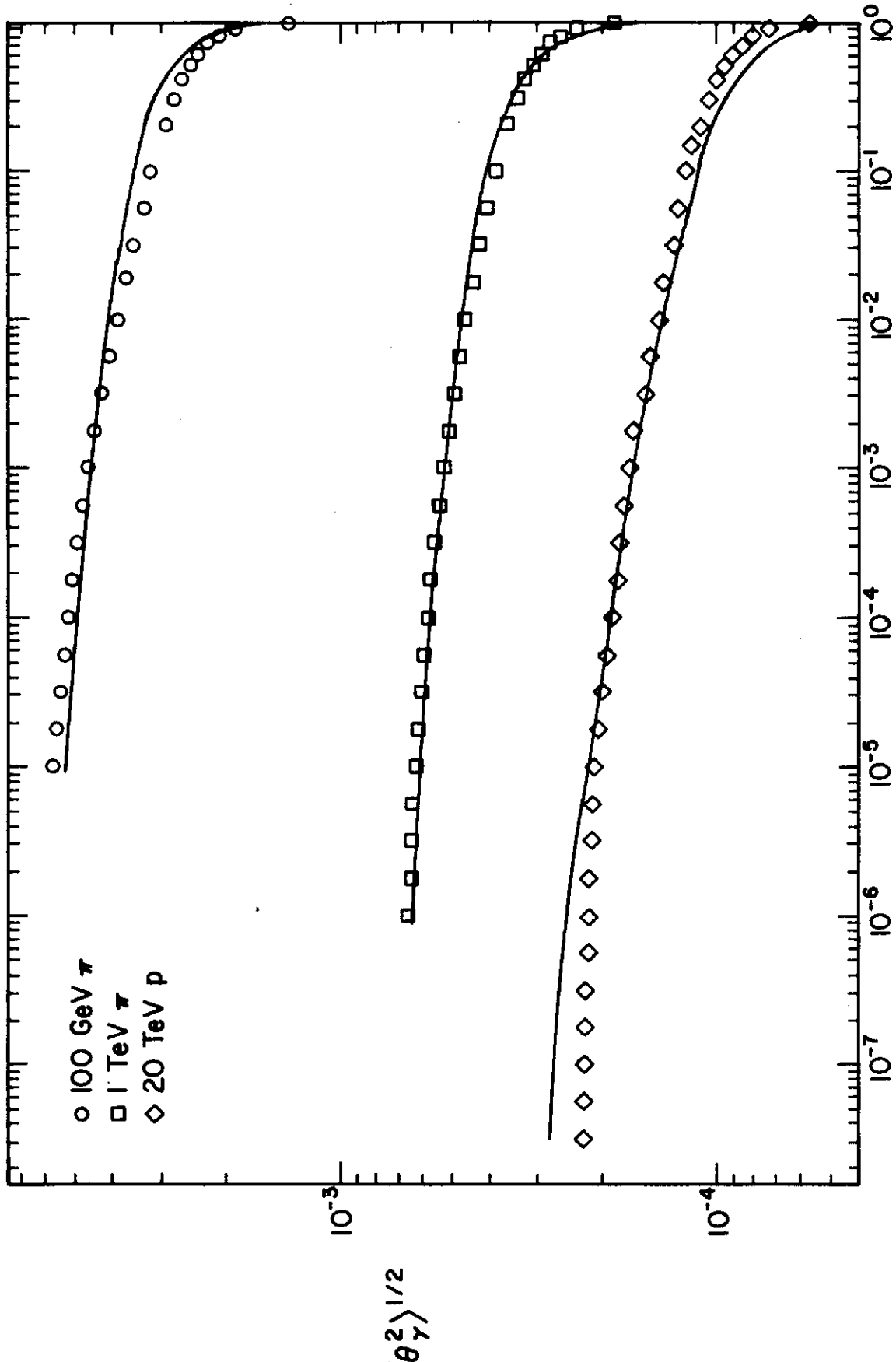
o 100 GeV π
□ 1 TeV π
◇ 20 TeV p
$\langle\theta_\gamma^2\rangle^{1/2}$
10^{-3}
10^{-4}
10^{-7}
10^{-6}
10^{-5}
10^{-4}
10^{-3}
10^{-2}
10^{-1}
10^{0}
ν

Fig. 3

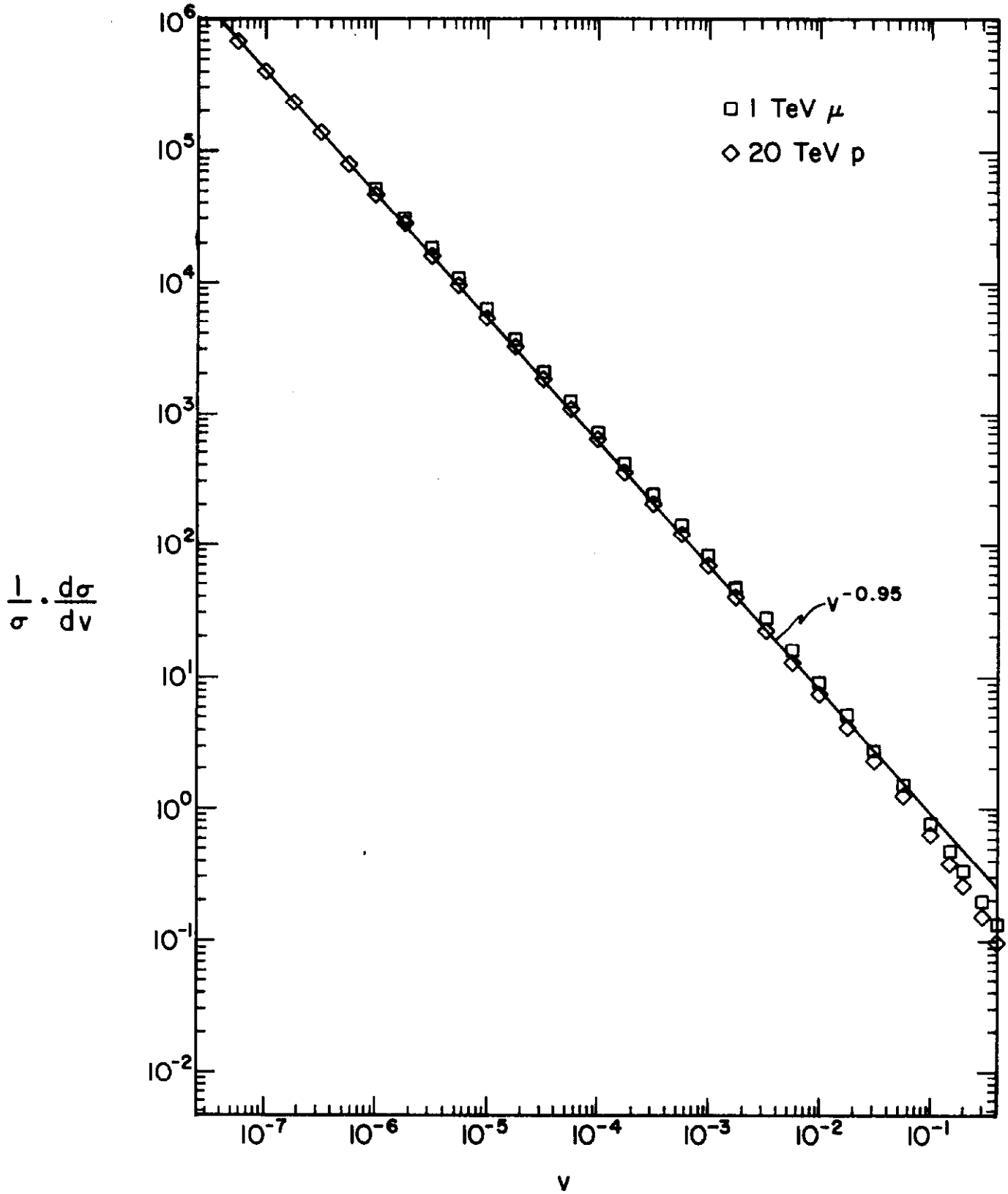

Fig. 4.a

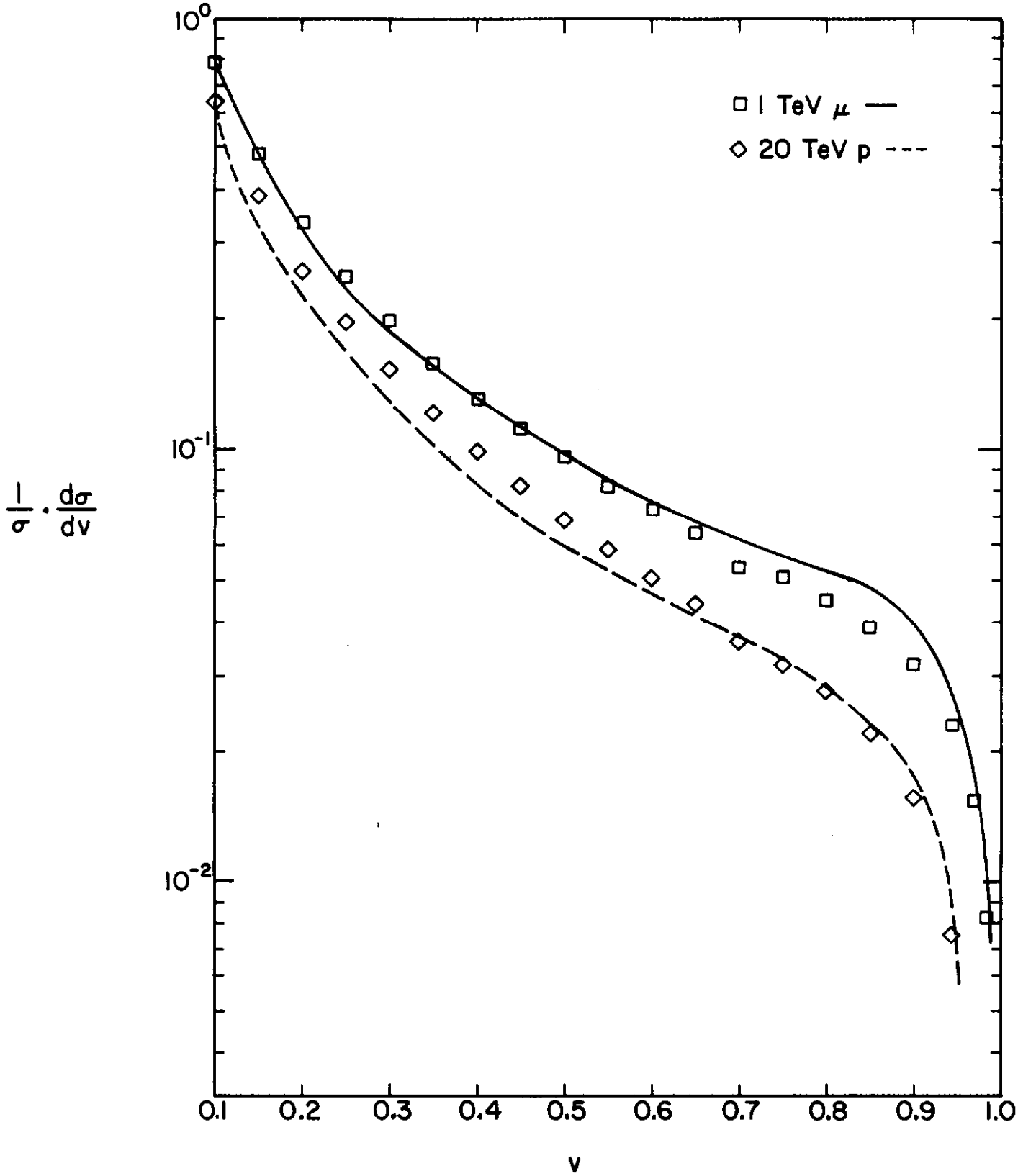
10^0
10^{-1}
10^{-2}
$\frac{1}{\sigma} \cdot \frac{d\sigma}{dv}$
□ 1 TeV μ
◇ 20 TeV p
0.1
0.2
0.3
0.4
0.5
0.6
0.7
0.8
0.9
1.0
v

Fig. 4.b

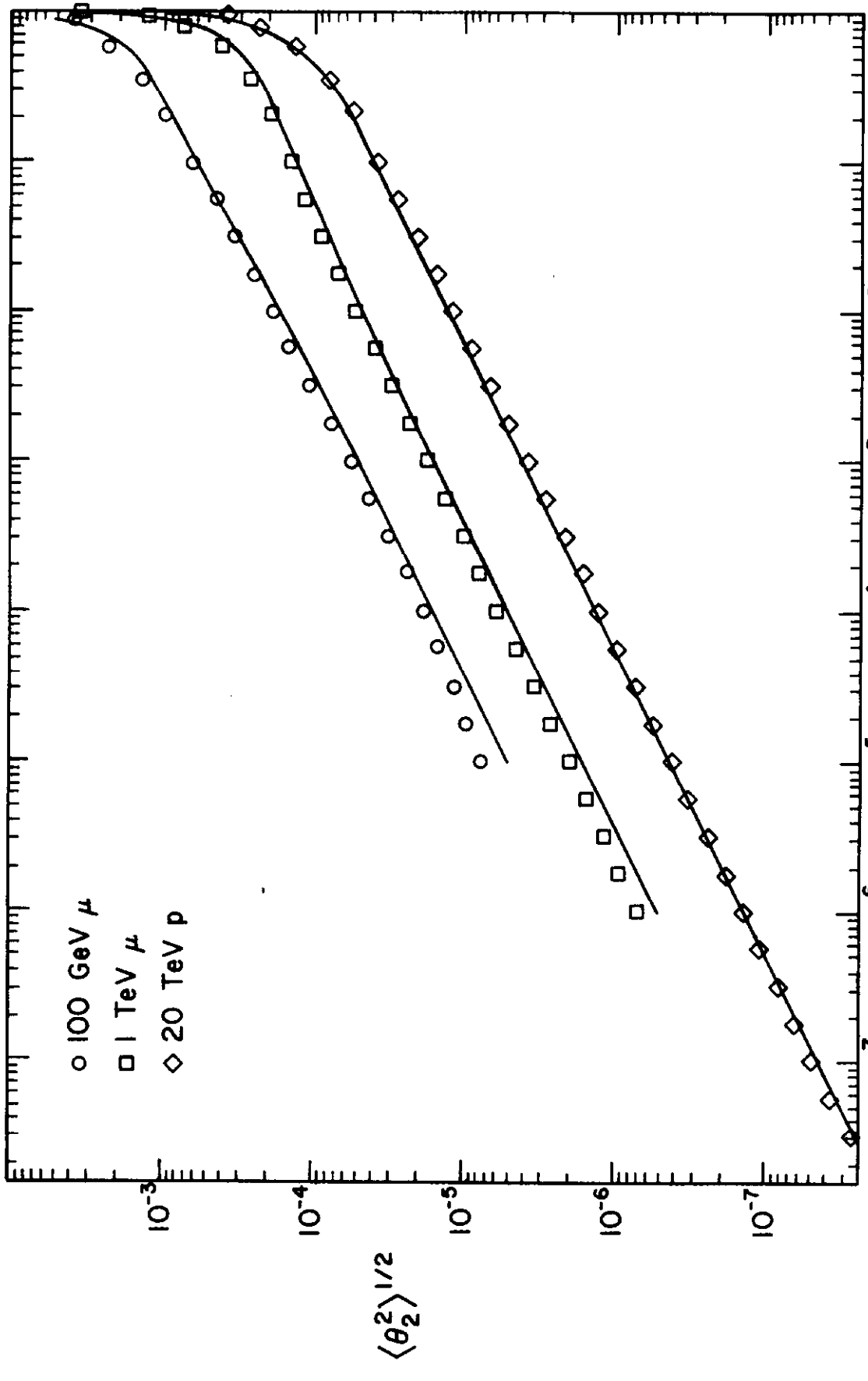
o 100 GeV μ
□ 1 TeV μ
◇ 20 TeV p
$\langle\theta_2^2\rangle^{1/2}$
10^{-3}
10^{-4}
10^{-5}
10^{-6}
10^{-7}
10^{-7}
10^{-6}
10^{-5}
10^{-4}
10^{-3}
10^{-2}
10^{-1}
v

Fig. 5

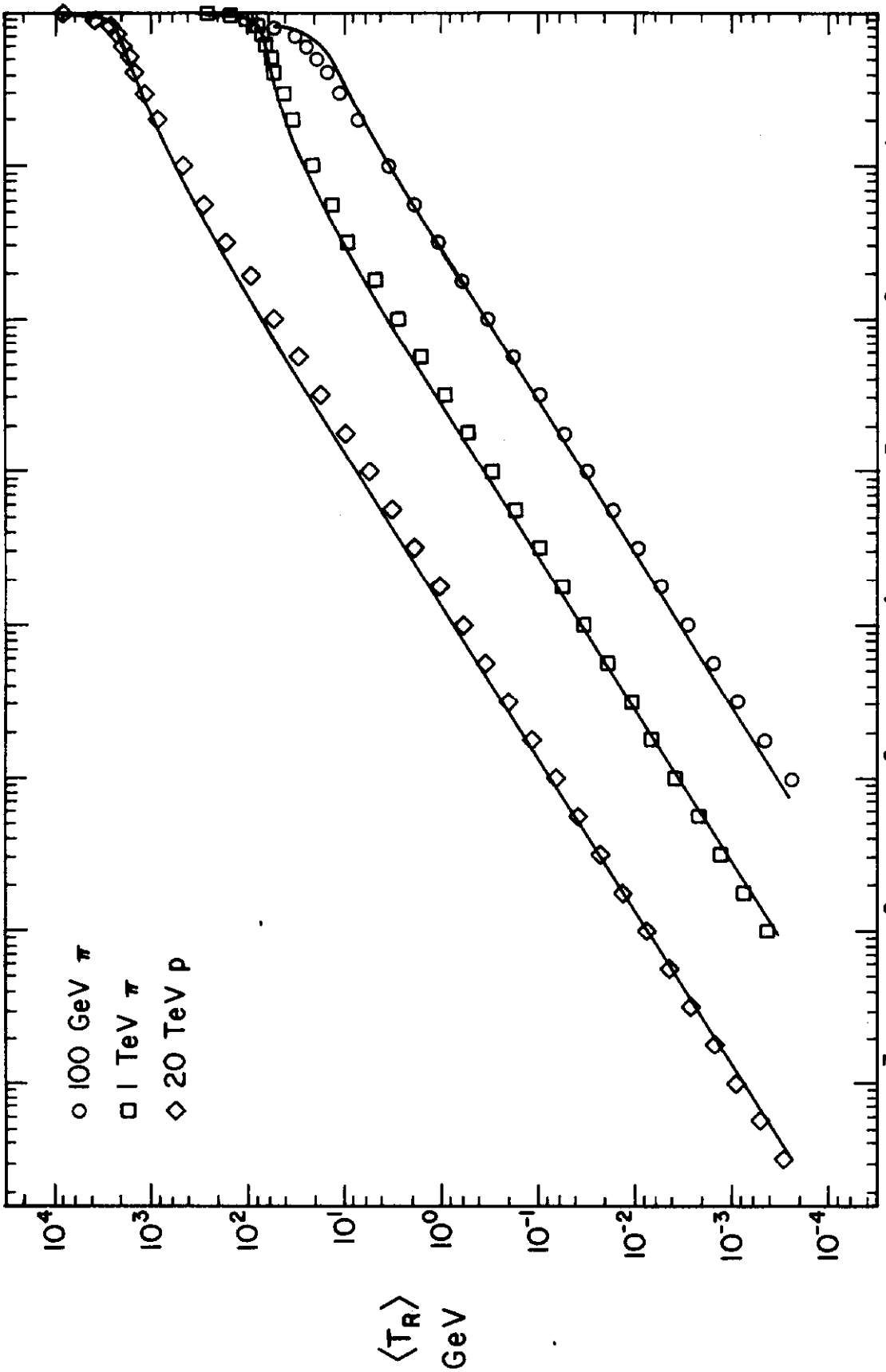

Fig. 6

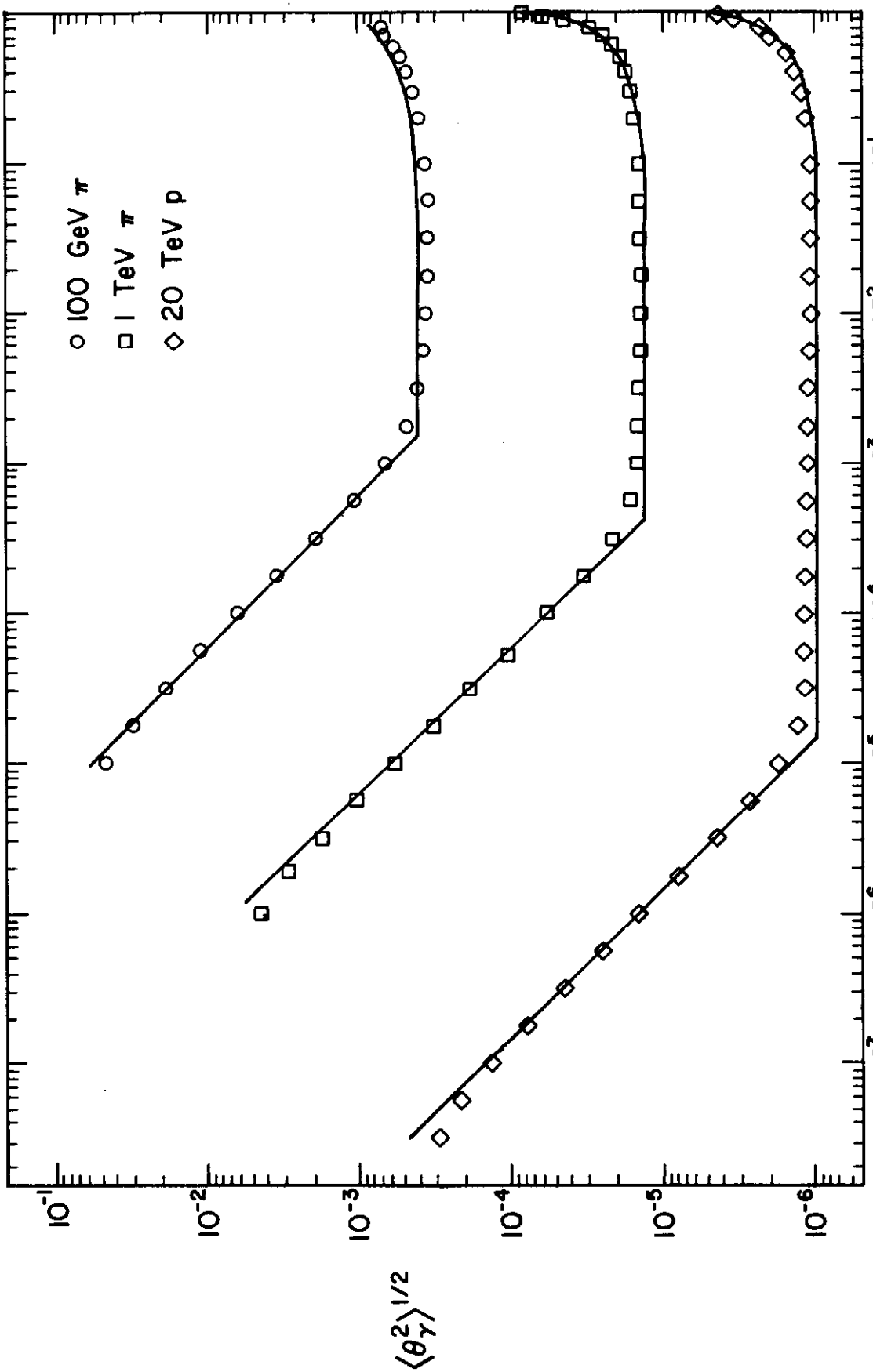
○ 100 GeV π
□ 1 TeV π
◇ 20 TeV p
$\langle\theta_\gamma^2\rangle^{1/2}$
10^{-1}
10^{-2}
10^{-3}
10^{-4}
10^{-5}
10^{-6}
10^{-7}
ν

Fig. 7

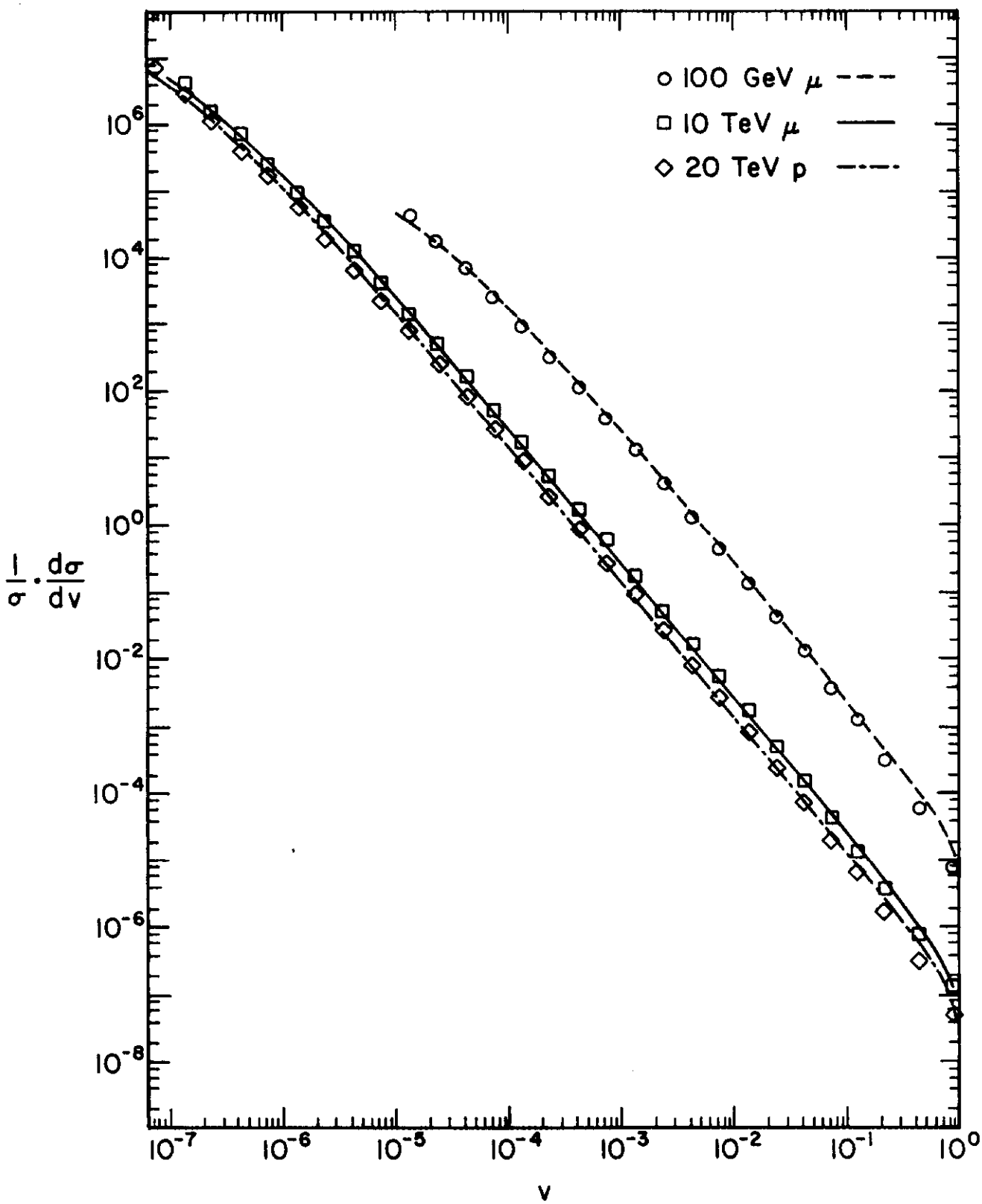
○ 100 GeV μ
□ 10 TeV μ
◇ 20 TeV p
$\frac{1}{\sigma}\cdot\frac{d\sigma}{dv}$
10^{6}
10^{4}
10^{2}
10^{0}
10^{-2}
10^{-4}
10^{-6}
10^{-8}
10^{-7}
10^{-6}
10^{-5}
10^{-4}
10^{-3}
10^{-2}
10^{-1}
10^{0}
v

Fig. 8

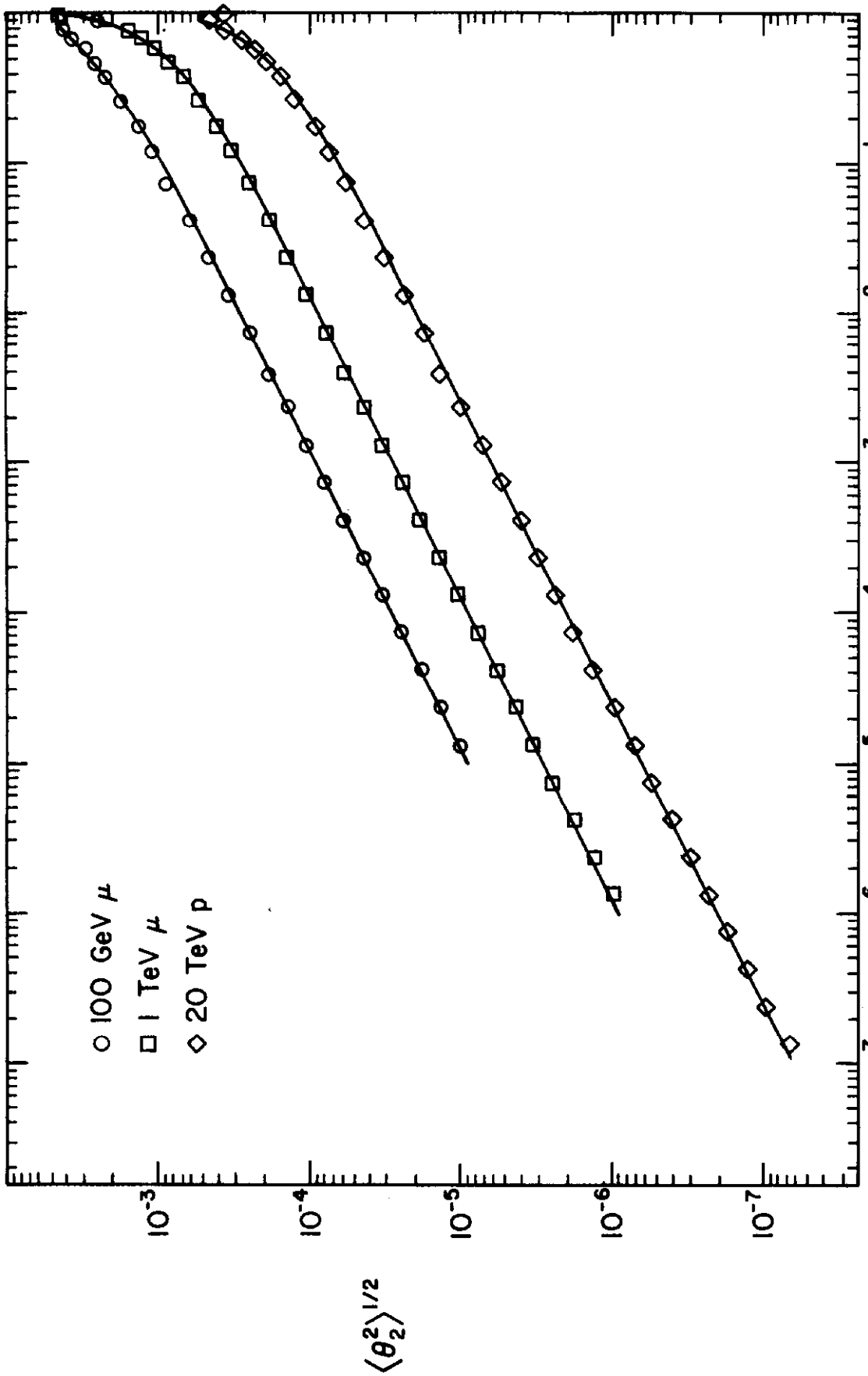
○ 100 GeV μ
□ 1 TeV μ
◇ 20 TeV p
$\langle\theta_2^2\rangle^{1/2}$
10^{-3}
10^{-4}
10^{-5}
10^{-6}
10^{-7}
10^{-7}
10^{-6}
10^{-5}
10^{-4}
10^{-3}
10^{-2}
10^{-1}
v

Fig. 9

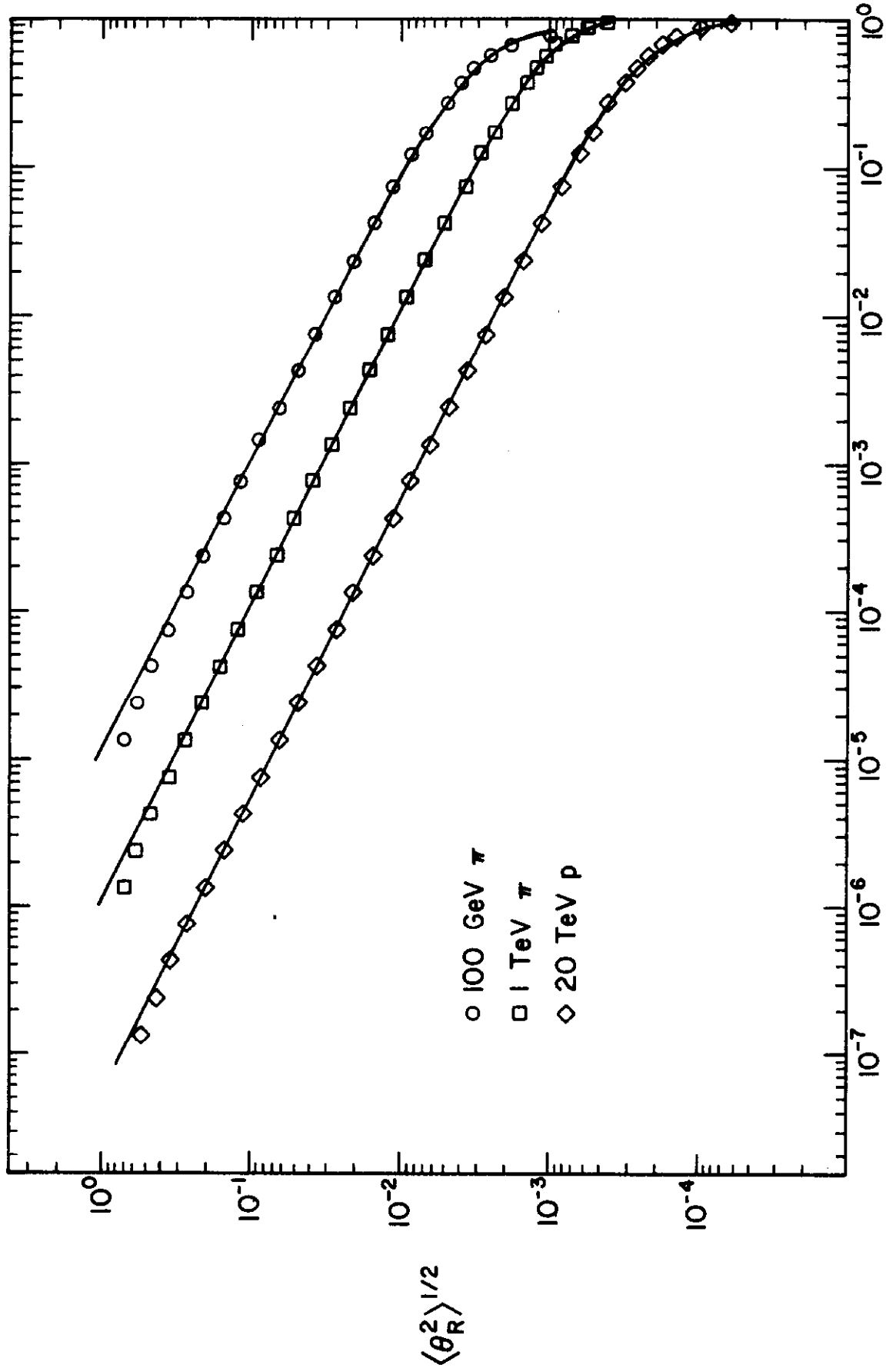
$\langle\theta_R^2\rangle^{1/2}$
10^0
10^{-1}
10^{-2}
10^{-3}
10^{-4}
10^{-5}
10^{-6}
10^{-7}
ν
○ 100 GeV π
□ 1 TeV π
◇ 20 TeV p

Fig. 10

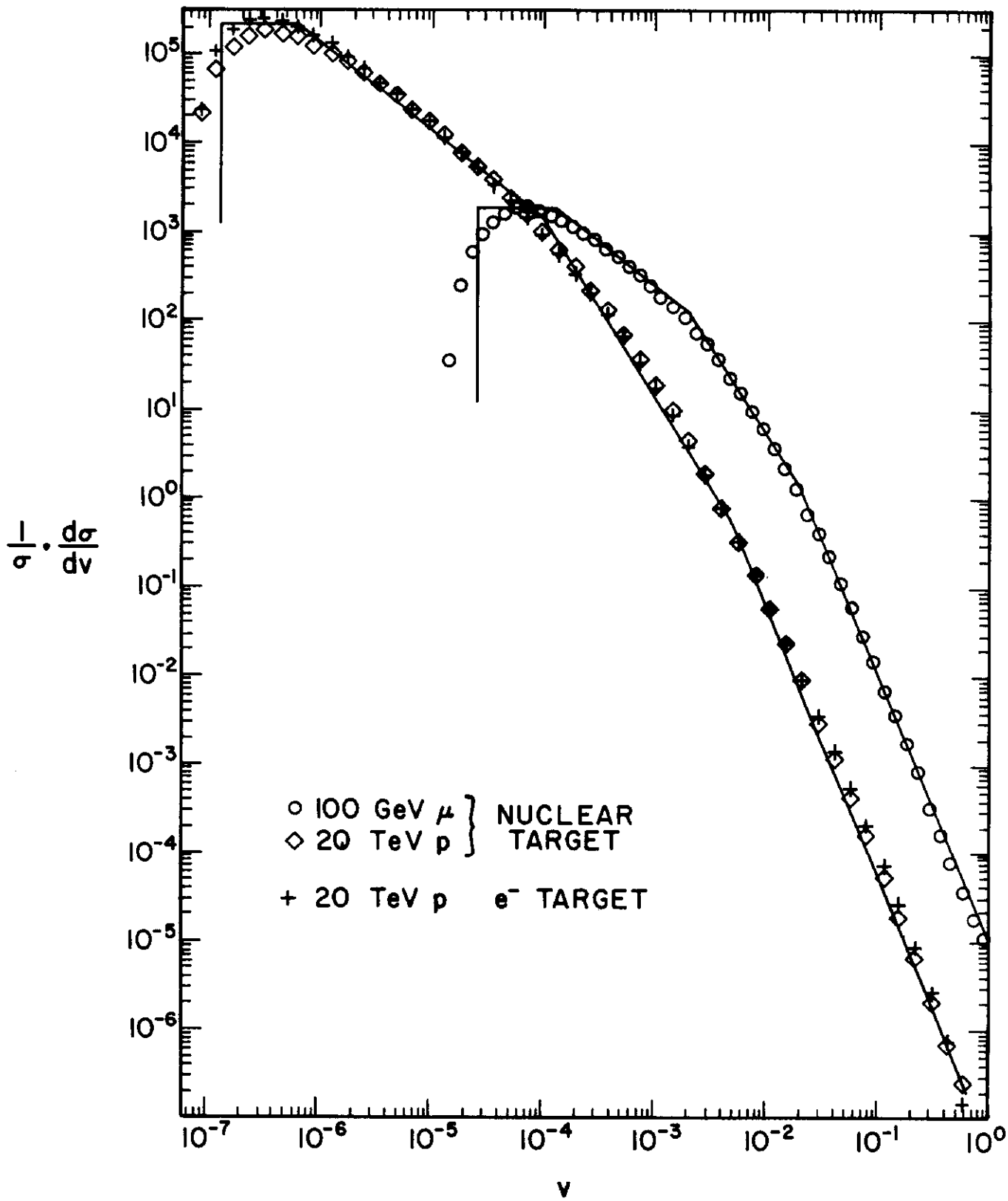
$\frac{1}{\sigma} \cdot \frac{d\sigma}{dv}$
10^5
10^4
10^3
10^2
10^1
10^0
10^{-1}
10^{-2}
10^{-3}
10^{-4}
10^{-5}
10^{-6}
○ 100 GeV μ } NUCLEAR
◇ 20 TeV p } TARGET
+ 20 TeV p e⁻ TARGET
10^{-7}
10^{-6}
10^{-5}
10^{-4}
10^{-3}
10^{-2}
10^{-1}
10^0
v

Fig. 11.a

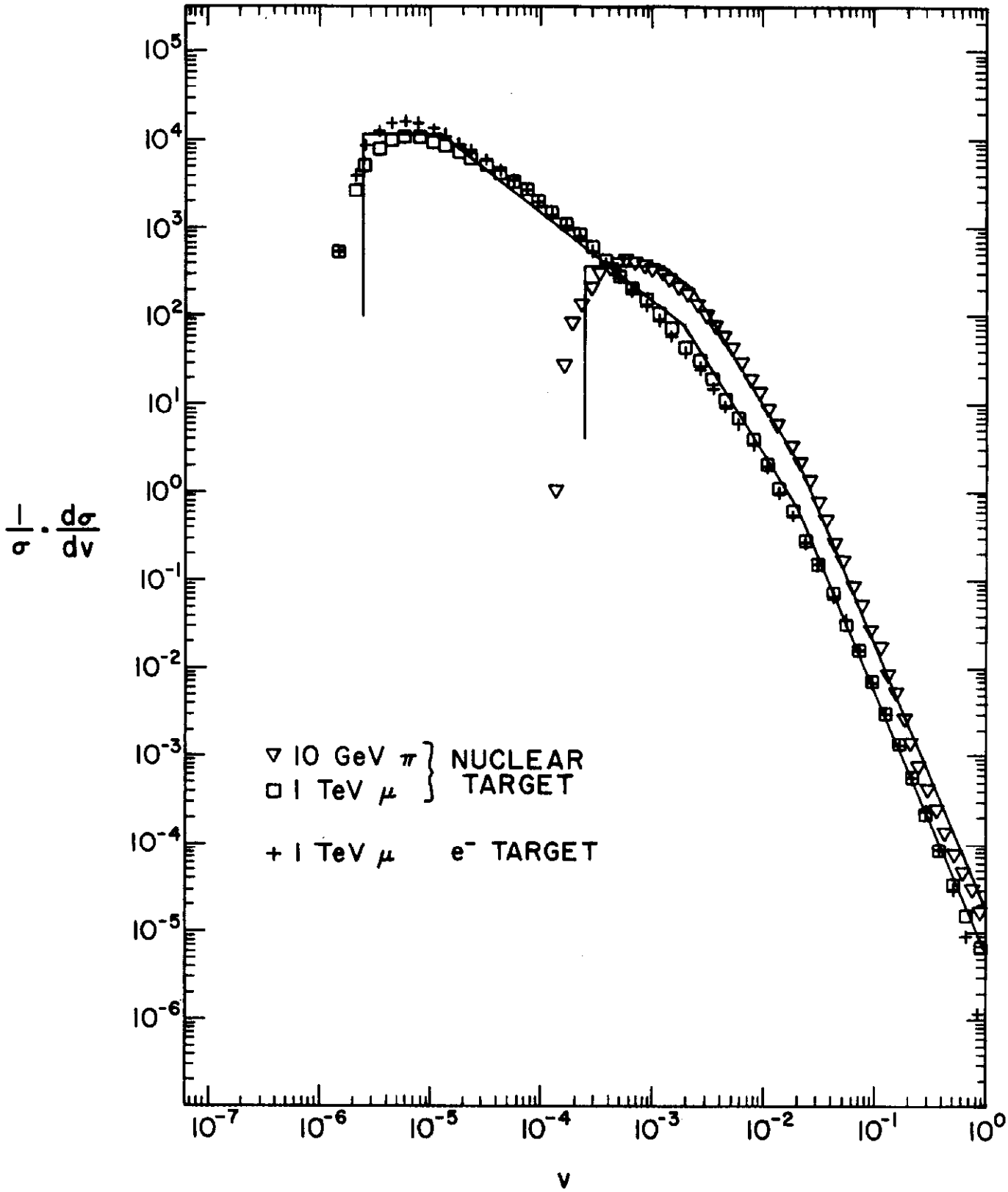
$\frac{1}{\sigma} \cdot \frac{d\sigma}{dv}$
10^5
10^4
10^3
10^2
10^1
10^0
10^{-1}
10^{-2}
10^{-3}
10^{-4}
10^{-5}
10^{-6}
▽ 10 GeV π } NUCLEAR
□ 1 TeV μ } TARGET
+ 1 TeV μ e⁻ TARGET
10^{-7}
10^{-6}
10^{-5}
10^{-4}
10^{-3}
10^{-2}
10^{-1}
10^0
v

Fig. 11.b

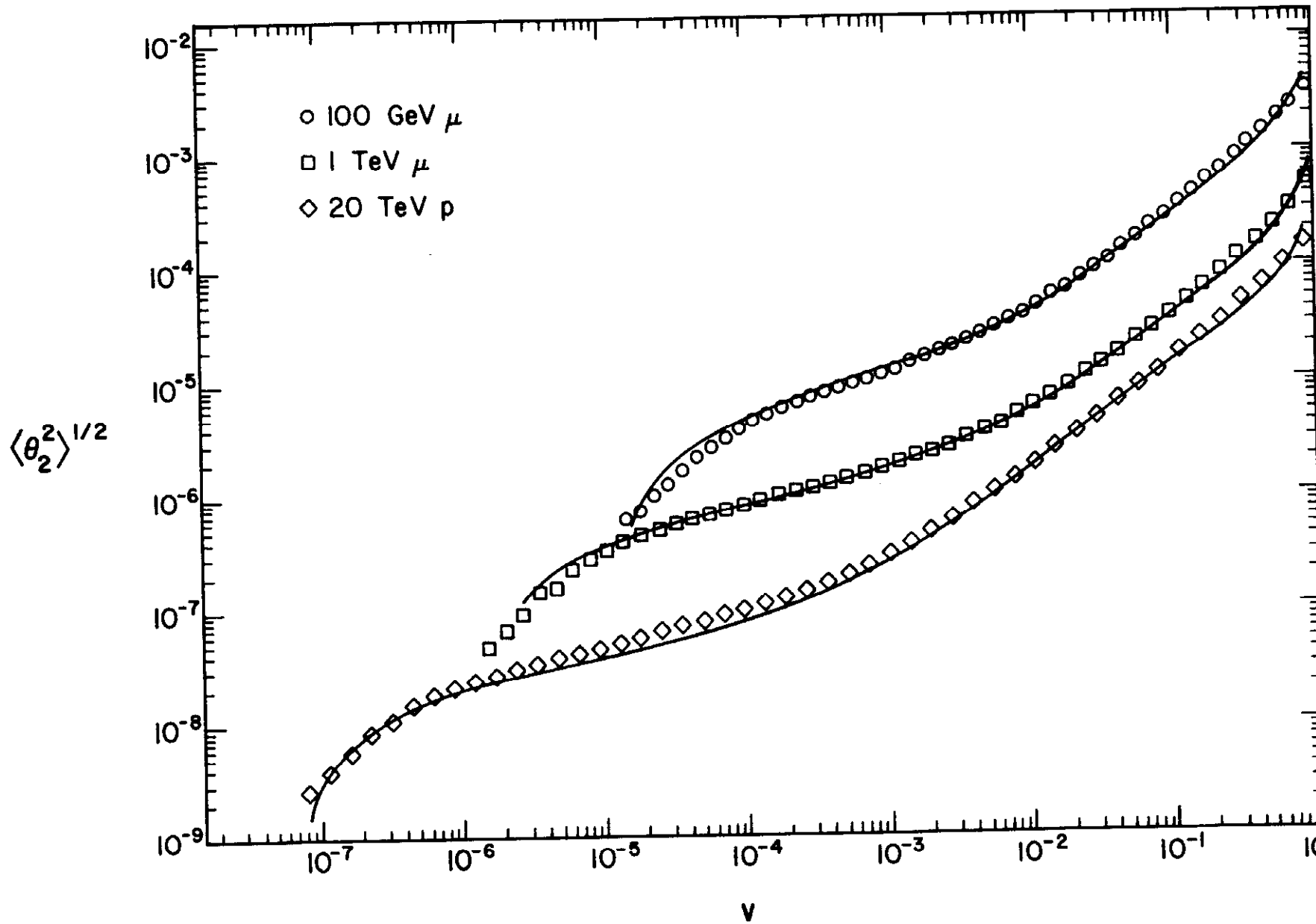
o 100 GeV μ
□ 1 TeV μ
◇ 20 TeV p
$\langle\theta_2^2\rangle^{1/2}$
10^{-2}
10^{-3}
10^{-4}
10^{-5}
10^{-6}
10^{-7}
10^{-8}
10^{-9}
10^{-7}
10^{-6}
10^{-5}
10^{-4}
10^{-3}
10^{-2}
10^{-1}
10^{0}
V

Fig. 12

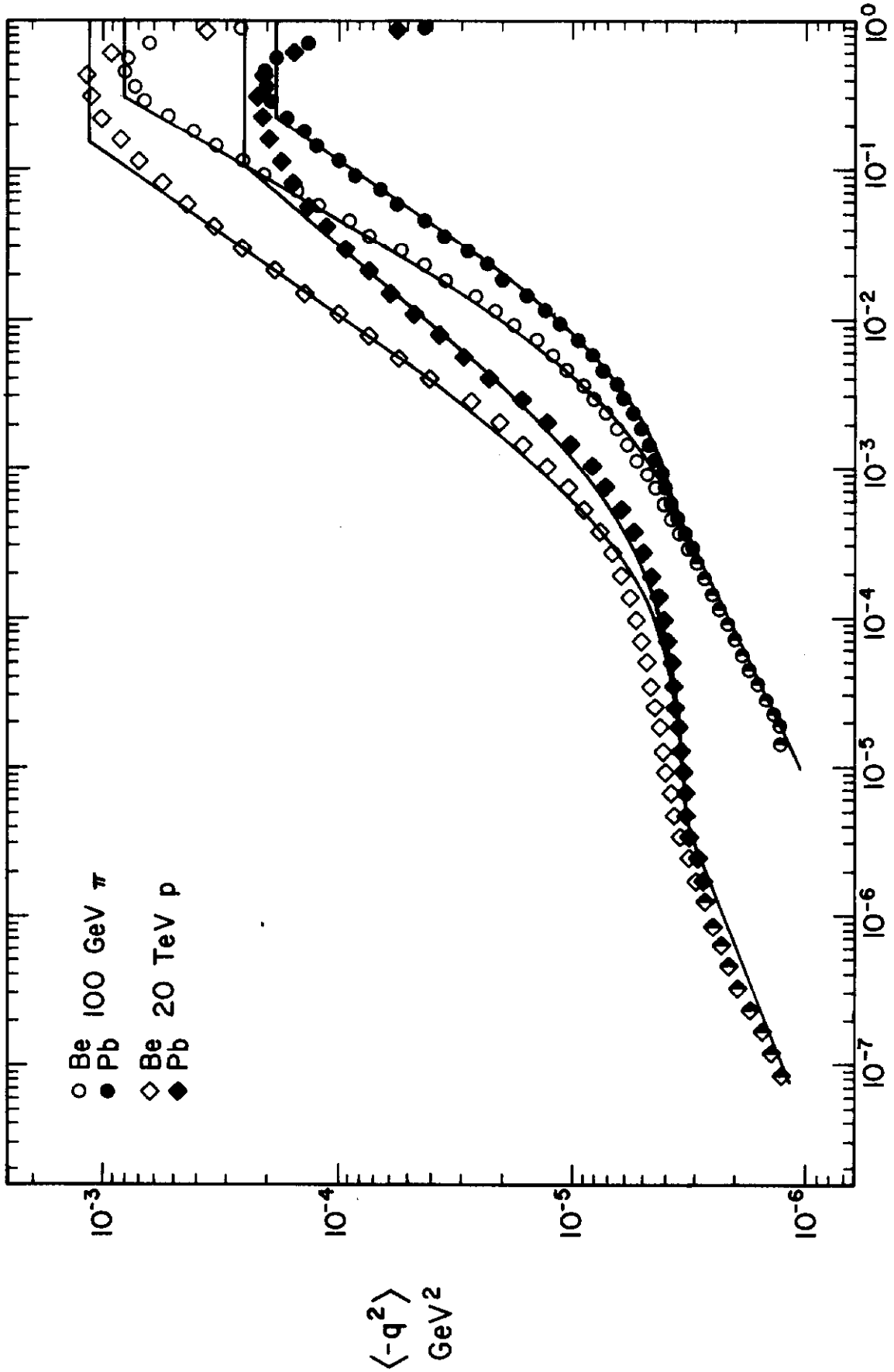
Be 100 GeV π
Pb
Be 20 TeV p
Pb
$\langle -q^2 \rangle$ GeV^2
10^{-3}
10^{-4}
10^{-5}
10^{-6}
10^{-7}
10^{-6}
10^{-5}
10^{-4}
10^{-3}
10^{-2}
10^{-1}
10^{0}
ν

Fig. 13

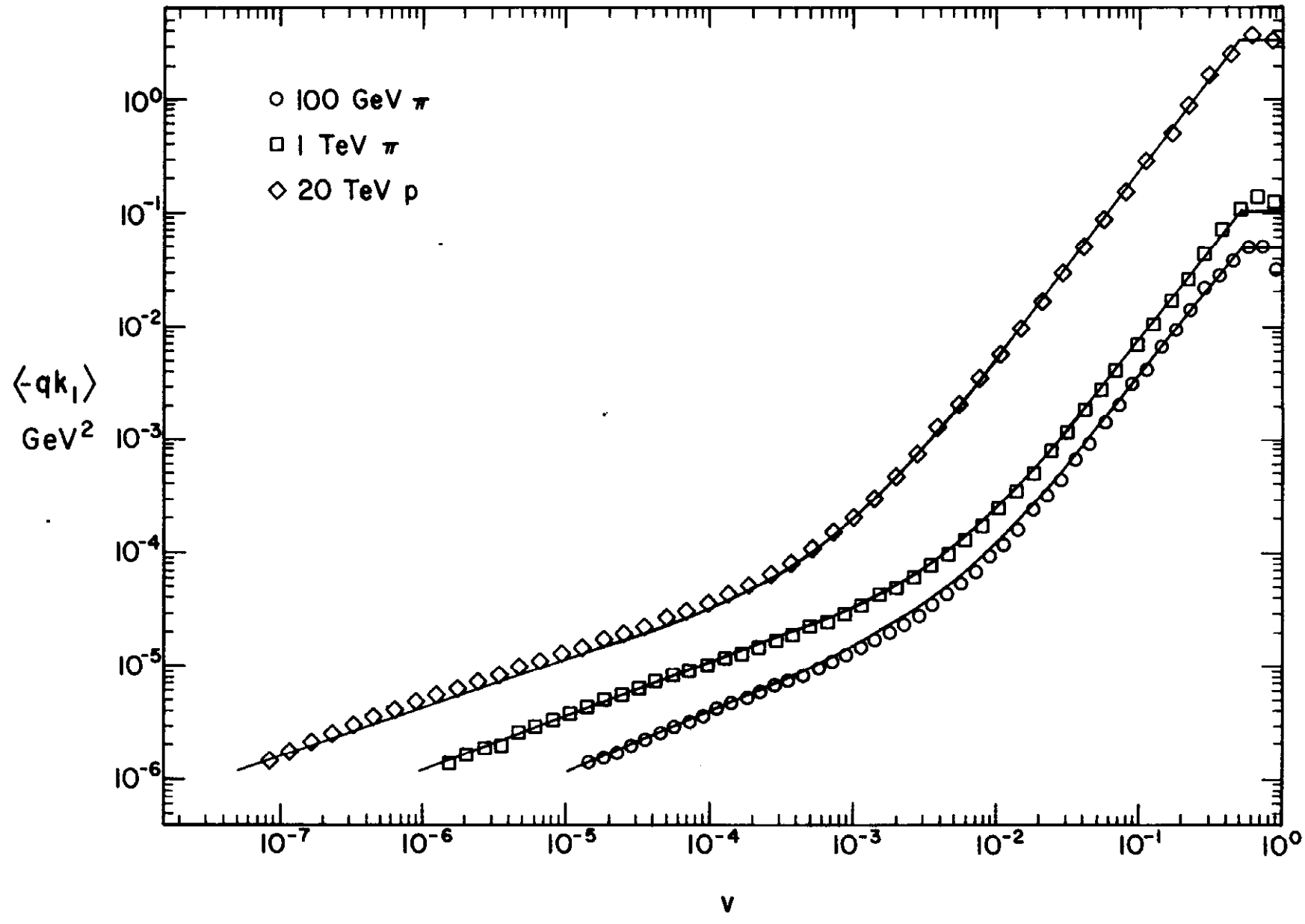
○ 100 GeV π
□ 1 TeV π
◇ 20 TeV p
$\langle -qk_1 \rangle$
GeV^2
10^0
10^{-1}
10^{-2}
10^{-3}
10^{-4}
10^{-5}
10^{-6}
10^{-7}
10^{-6}
10^{-5}
10^{-4}
10^{-3}
10^{-2}
10^{-1}
10^0
v

Fig. 14

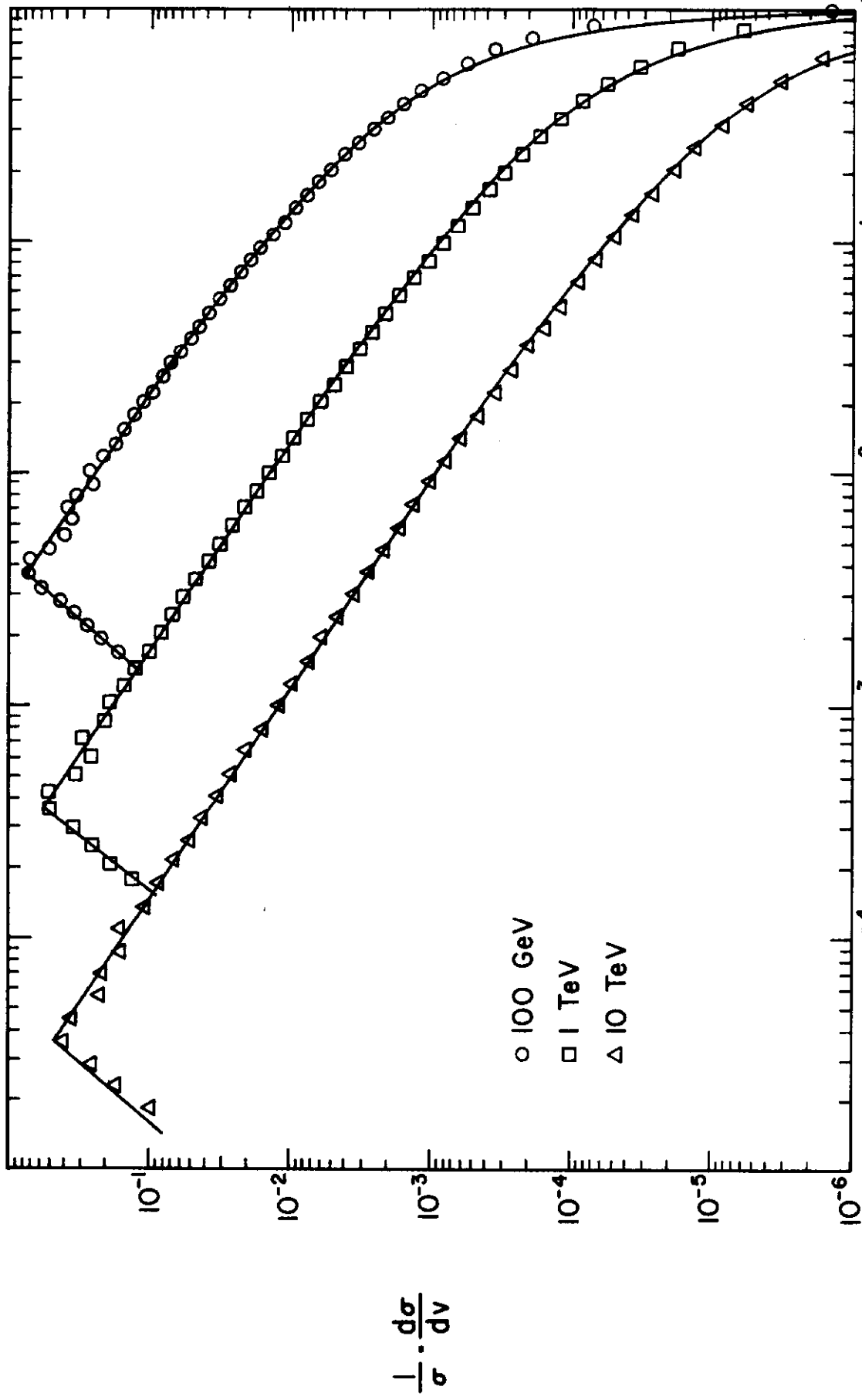
$\frac{1}{\sigma} \cdot \frac{d\sigma}{dv}$
10^{-1}
10^{-2}
10^{-3}
10^{-4}
10^{-5}
10^{-6}
10^{0}
10^{-1}
10^{-2}
10^{-3}
10^{-4}
v
o 100 GeV
□ 1 TeV
△ 10 TeV

Fig. 15

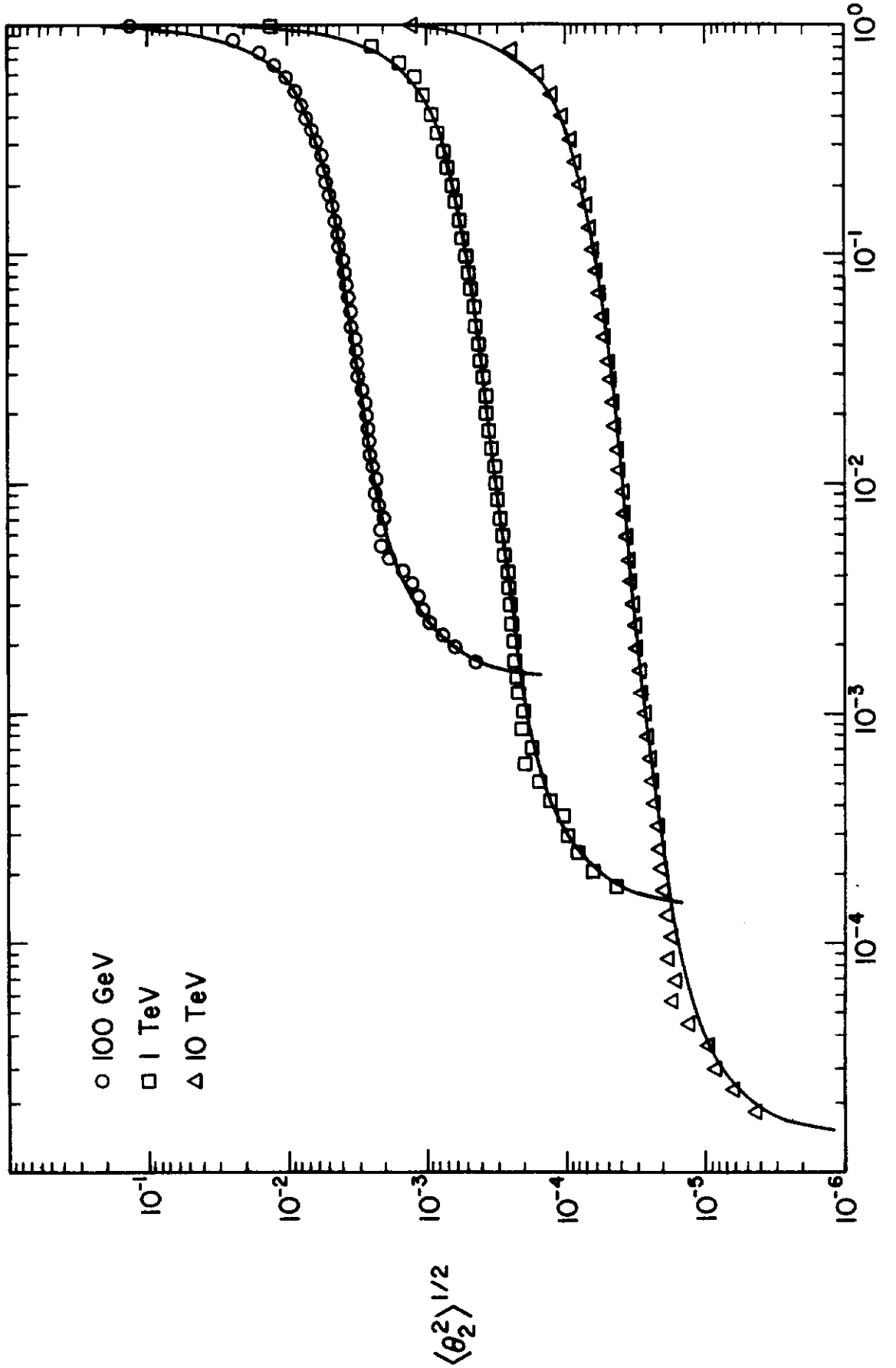
o 100 GeV
□ 1 TeV
△ 10 TeV
$\langle\theta_2^2\rangle^{1/2}$
10^{-1}
10^{-2}
10^{-3}
10^{-4}
10^{-5}
10^{-6}
10^{0}
10^{-1}
10^{-2}
10^{-3}
10^{-4}
v

Fig. 16

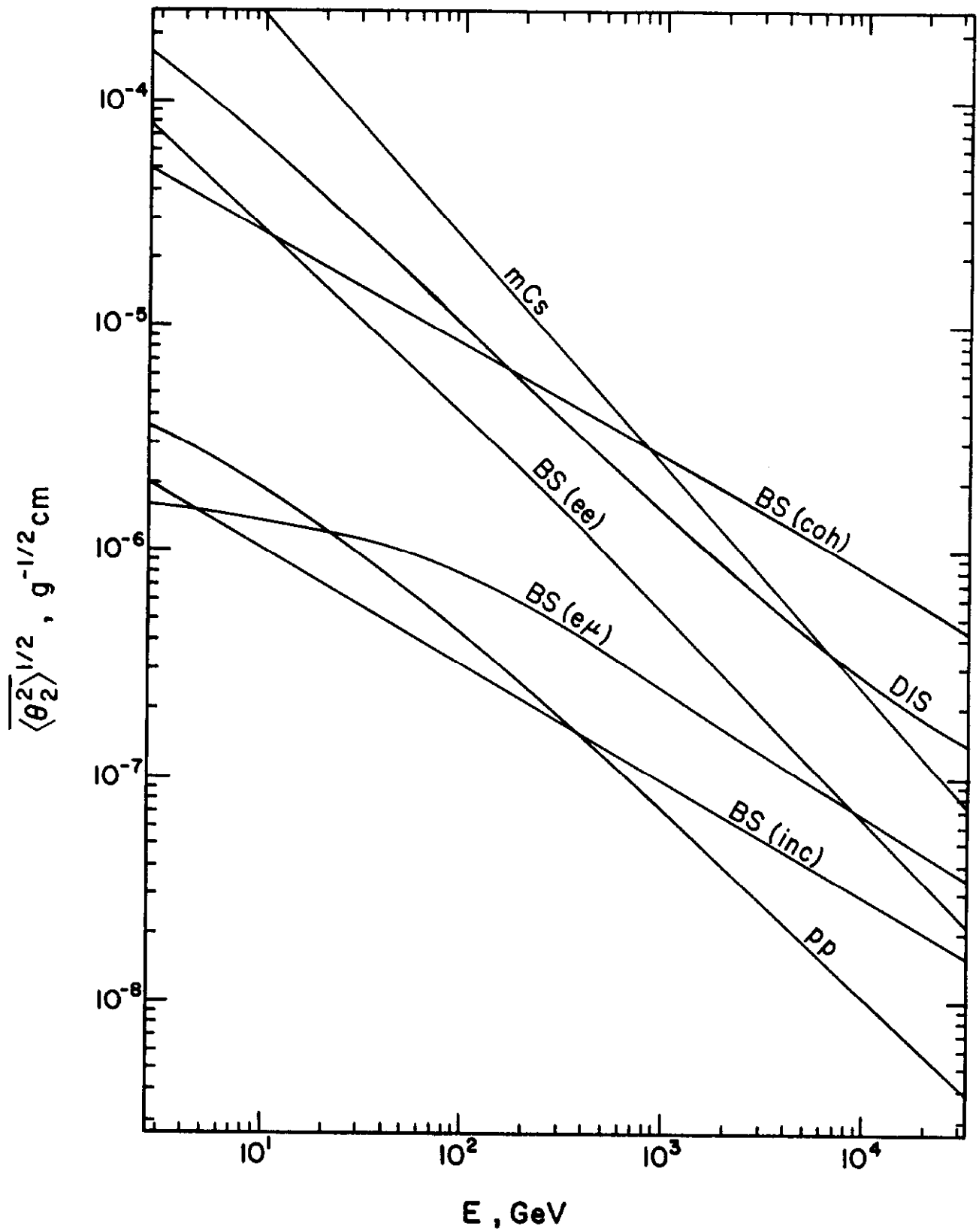
10^{-4}
10^{-5}
10^{-6}
10^{-7}
10^{-8}
$\overline{\langle\theta_2^2\rangle}^{1/2}$, $g^{-1/2}cm$
mCs
BS (ee)
BS (coh)
BS (eμ)
DIS
BS (inc)
pp
10^1
10^2
10^3
10^4
E , GeV

Fig. 17.a

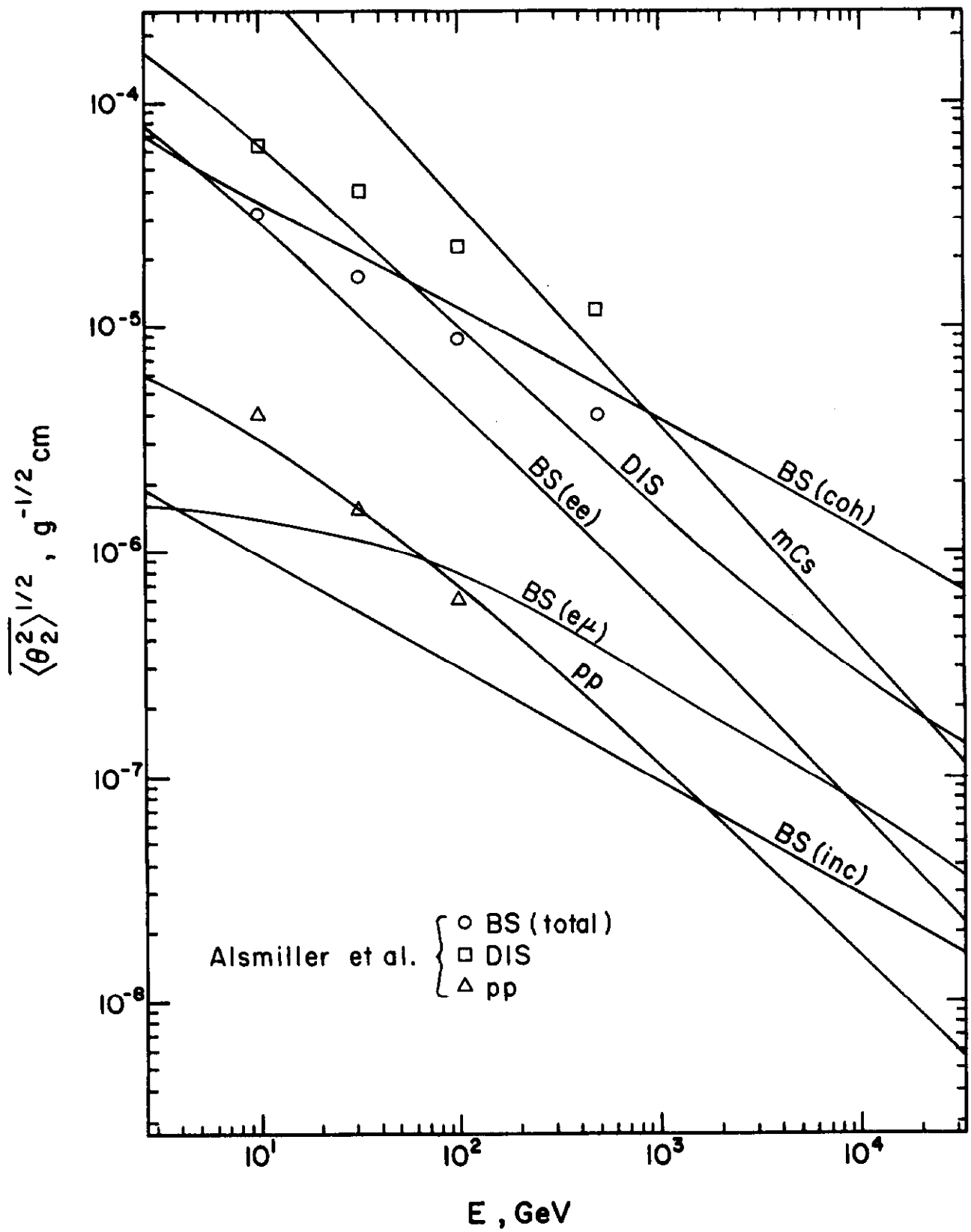
$\overline{\langle\theta_2^2\rangle}^{1/2}$, $g^{-1/2}$ cm
10^{-4}
10^{-5}
10^{-6}
10^{-7}
10^{-8}
10^1
10^2
10^3
10^4
E , GeV
BS(ee)
DIS
mCs
BS(coh)
BS(eμ)
pp
BS(inc)
Alsmiller et al.
BS (total)
DIS
pp

Fig. 17.b

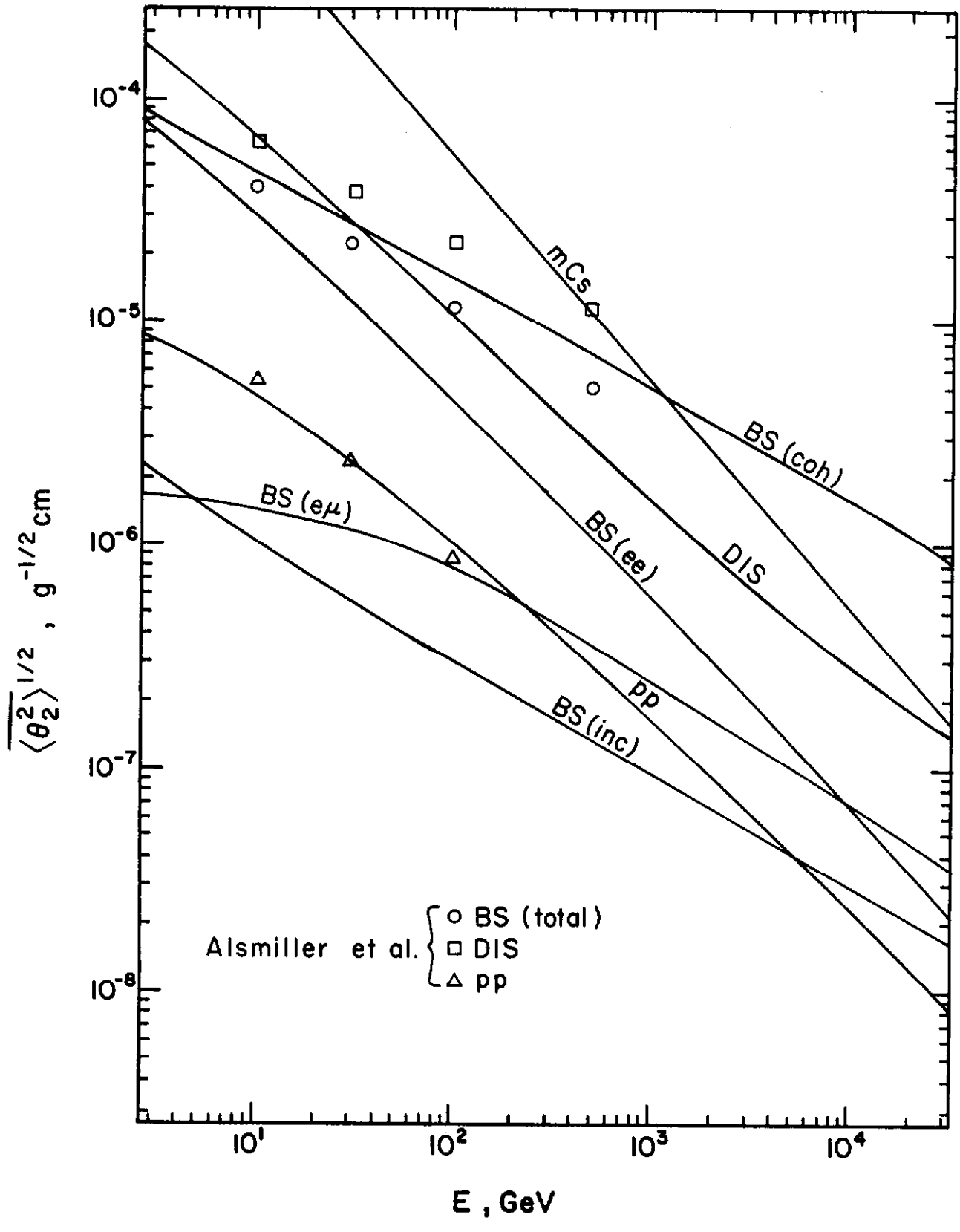
10^{-4}
10^{-5}
10^{-6}
10^{-7}
10^{-8}
$\overline{\langle\theta_2^2\rangle}^{1/2}$, $g^{-1/2}$ cm
mCs
BS (coh)
BS (eμ)
BS (ee)
DIS
pp
BS (inc)
Alsmiller et al.
BS (total)
DIS
pp
10^1
10^2
10^3
10^4
E , GeV

Fig. 17.c

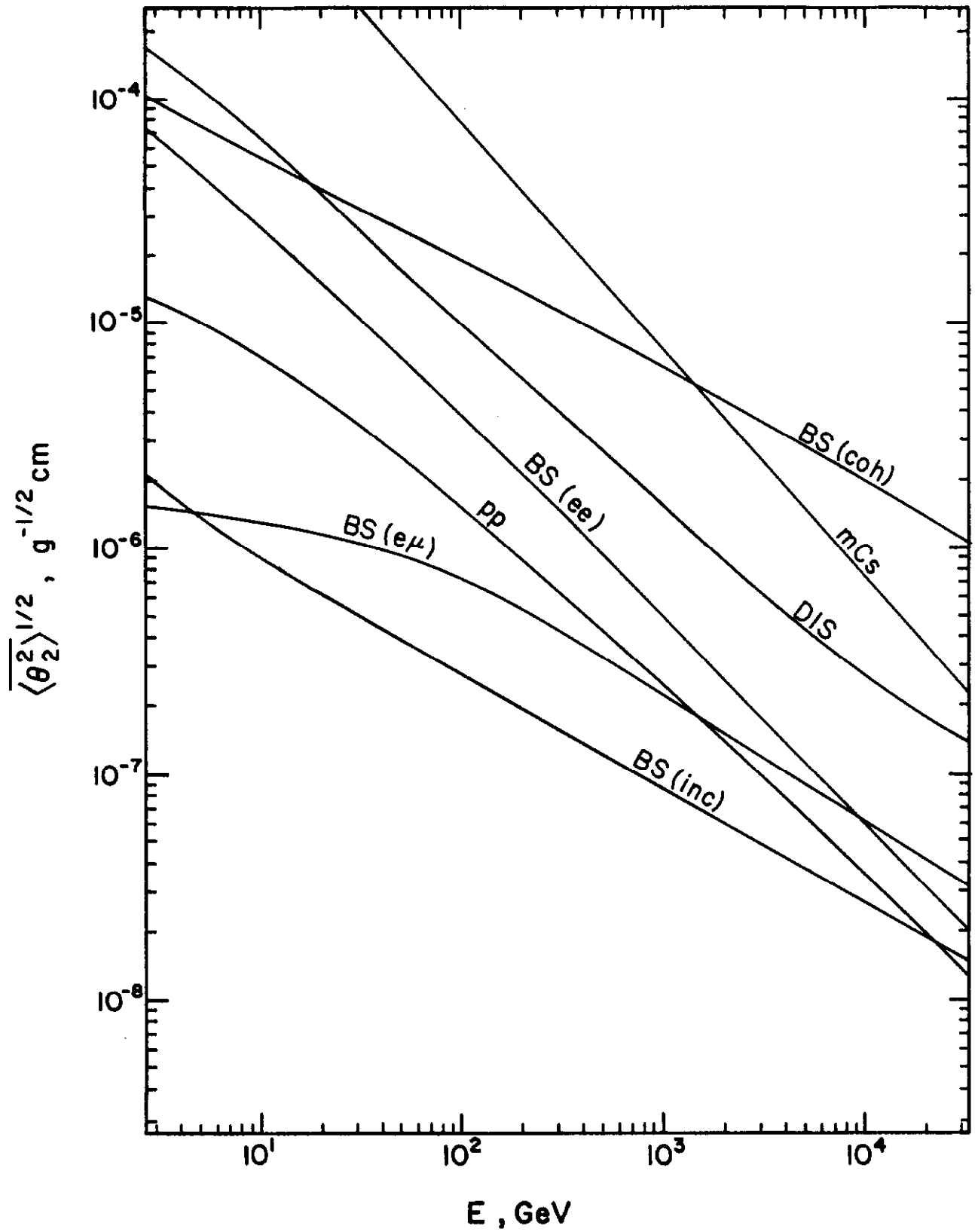
10^{-4}
10^{-5}
10^{-6}
10^{-7}
10^{-8}
$\overline{\langle\theta_2^2\rangle}^{1/2}$, $g^{-1/2}$ cm
BS (coh)
BS (ee)
BS (eμ)
pp
mCs
DIS
BS (inc)
10^1
10^2
10^3
10^4
E , GeV

Fig. 17.d

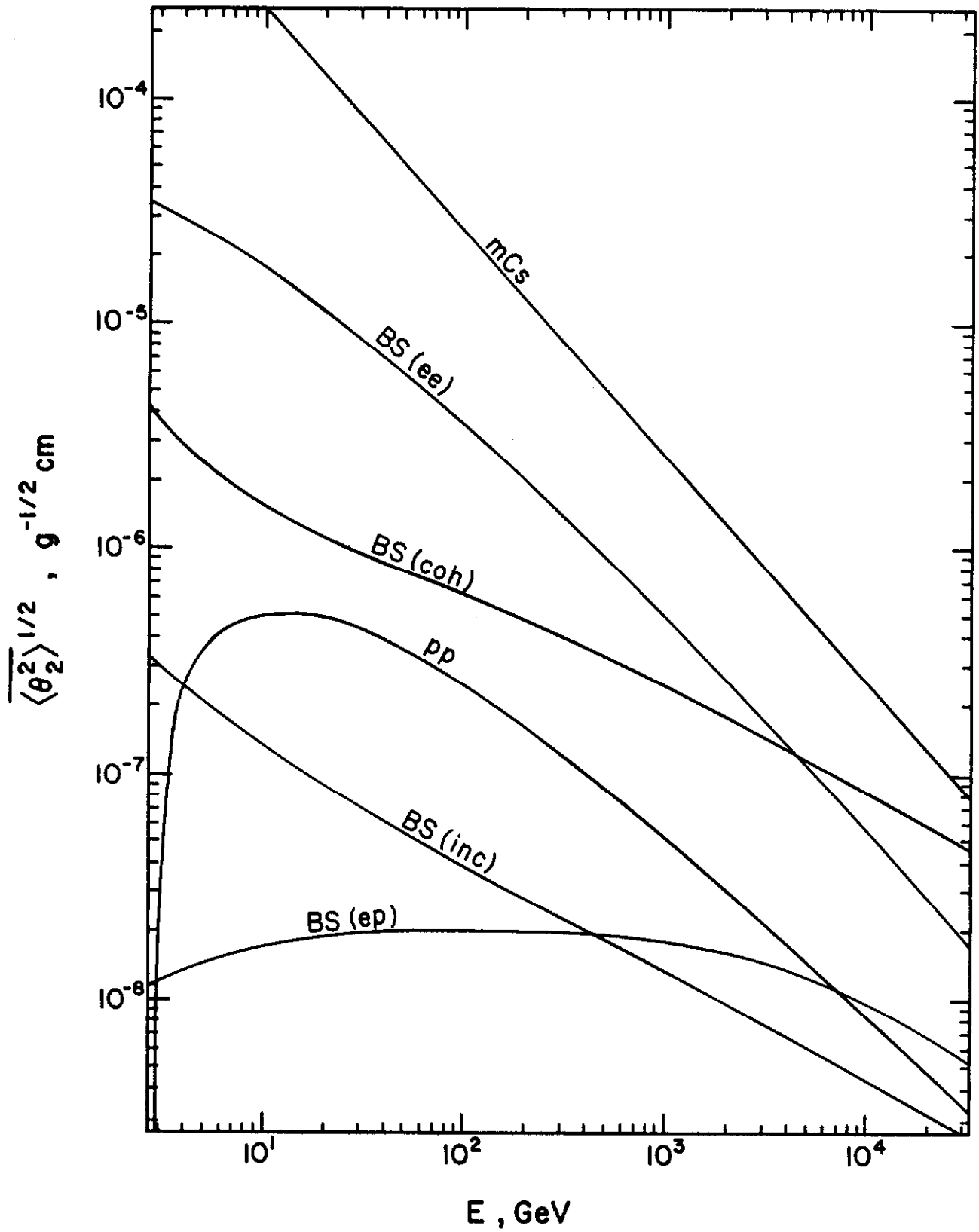
mCs
BS (ee)
BS (coh)
pp
BS (inc)
BS (ep)
10^{-4}
10^{-5}
10^{-6}
10^{-7}
10^{-8}
10^{1}
10^{2}
10^{3}
10^{4}
$\overline{\langle \theta_2^2 \rangle}^{1/2}$, $g^{-1/2}$ cm
E , GeV

Fig. 18.a

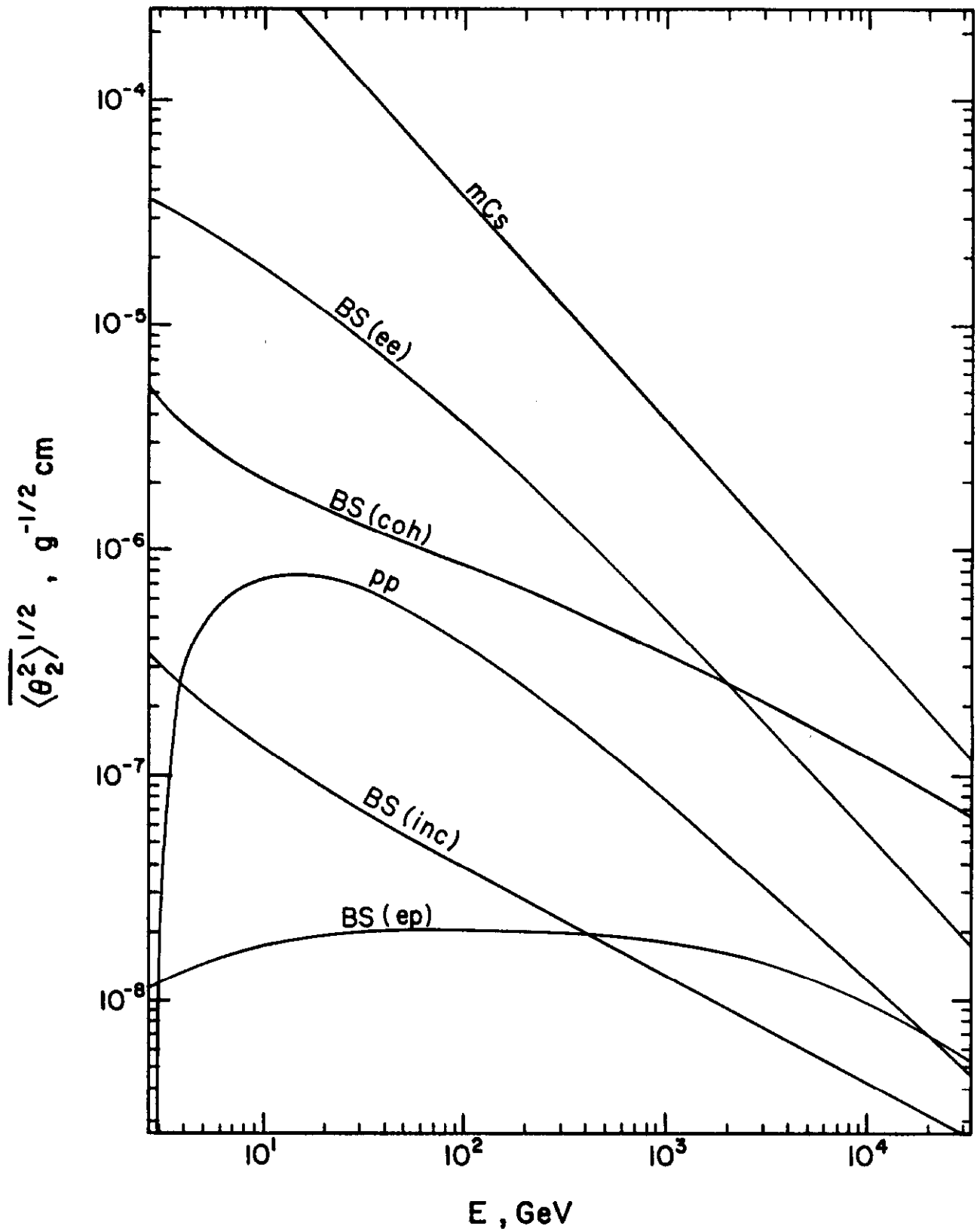
10^{-4}
10^{-5}
10^{-6}
10^{-7}
10^{-8}
$\overline{\langle\theta_2^2\rangle}^{1/2}$, $g^{-1/2}$ cm
mCs
BS (ee)
BS (coh)
pp
BS (inc)
BS (ep)
10^1
10^2
10^3
10^4
E , GeV

Fig. 18. b

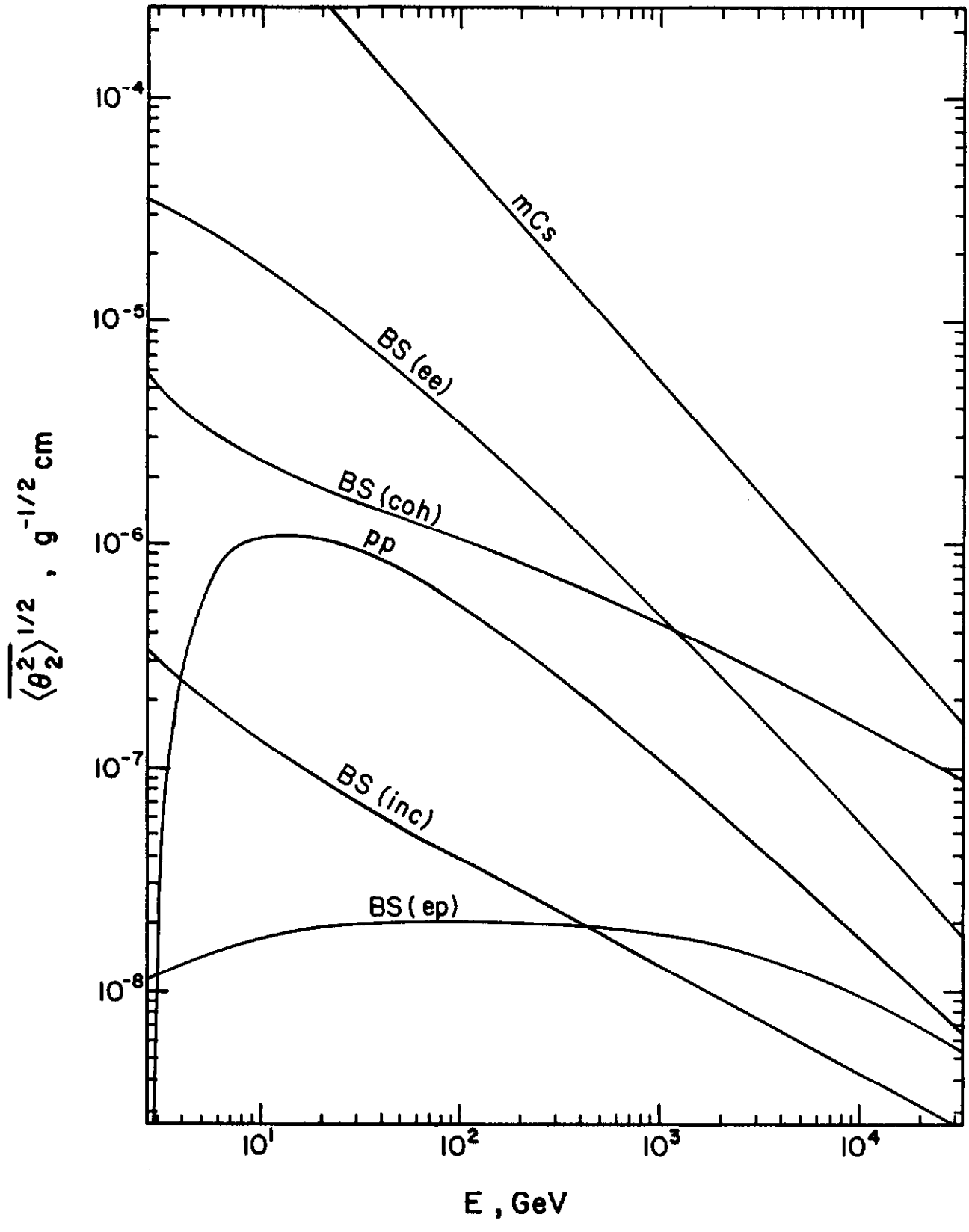
mCs
BS (ee)
BS (coh)
pp
BS (inc)
BS (ep)
10^{-4}
10^{-5}
10^{-6}
10^{-7}
10^{-8}
10^{1}
10^{2}
10^{3}
10^{4}
$\overline{\langle\theta_2^2\rangle}^{1/2}$, $g^{-1/2}$ cm
E , GeV

Fig. 18.c

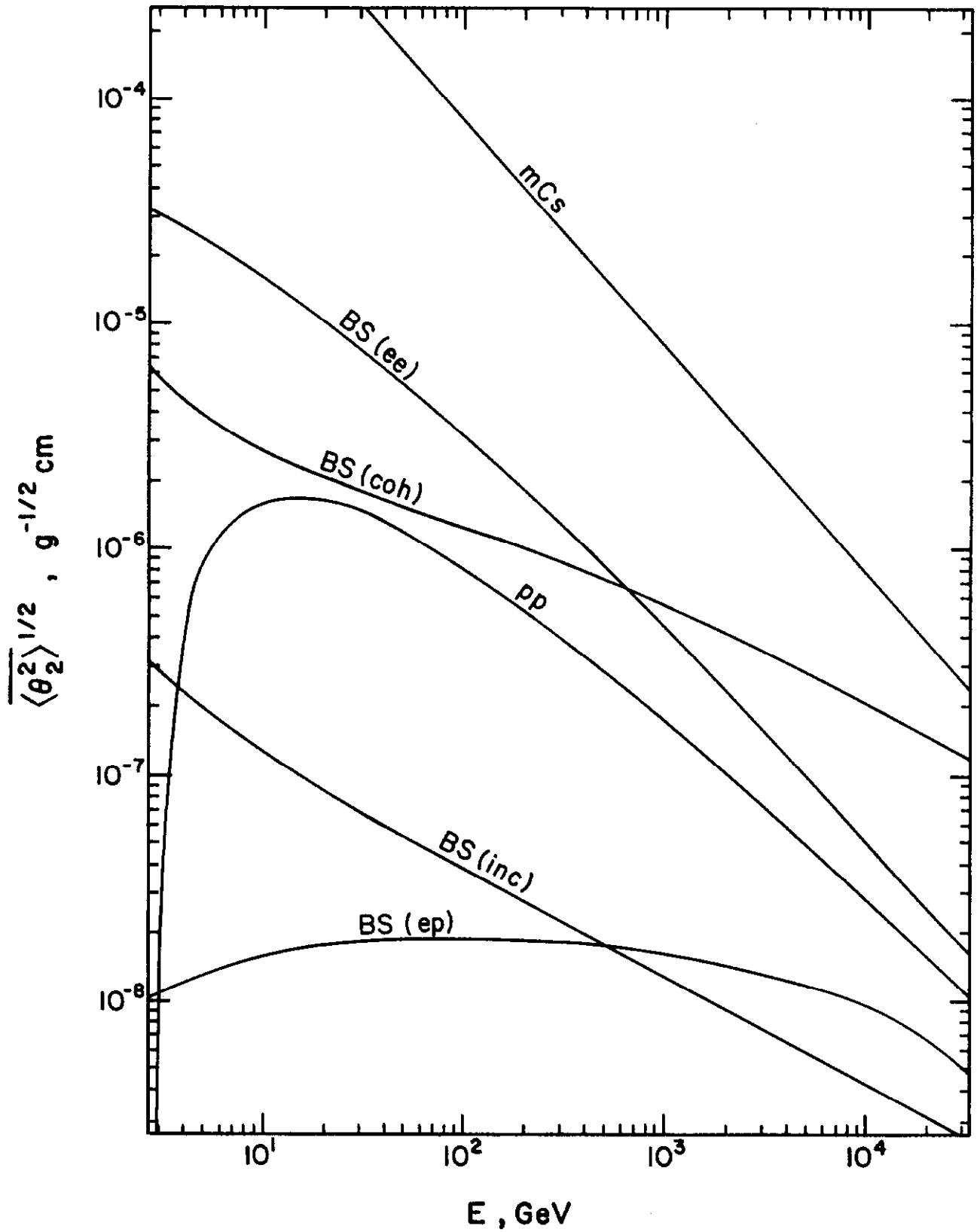
mCs
BS (ee)
BS (coh)
pp
BS (inc)
BS (ep)
10^{-4}
10^{-5}
10^{-6}
10^{-7}
10^{-8}
10^{1}
10^{2}
10^{3}
10^{4}
$\overline{\langle \theta_2^2 \rangle}^{1/2}$, $g^{-1/2}$ cm
E , GeV

Fig. 18.d

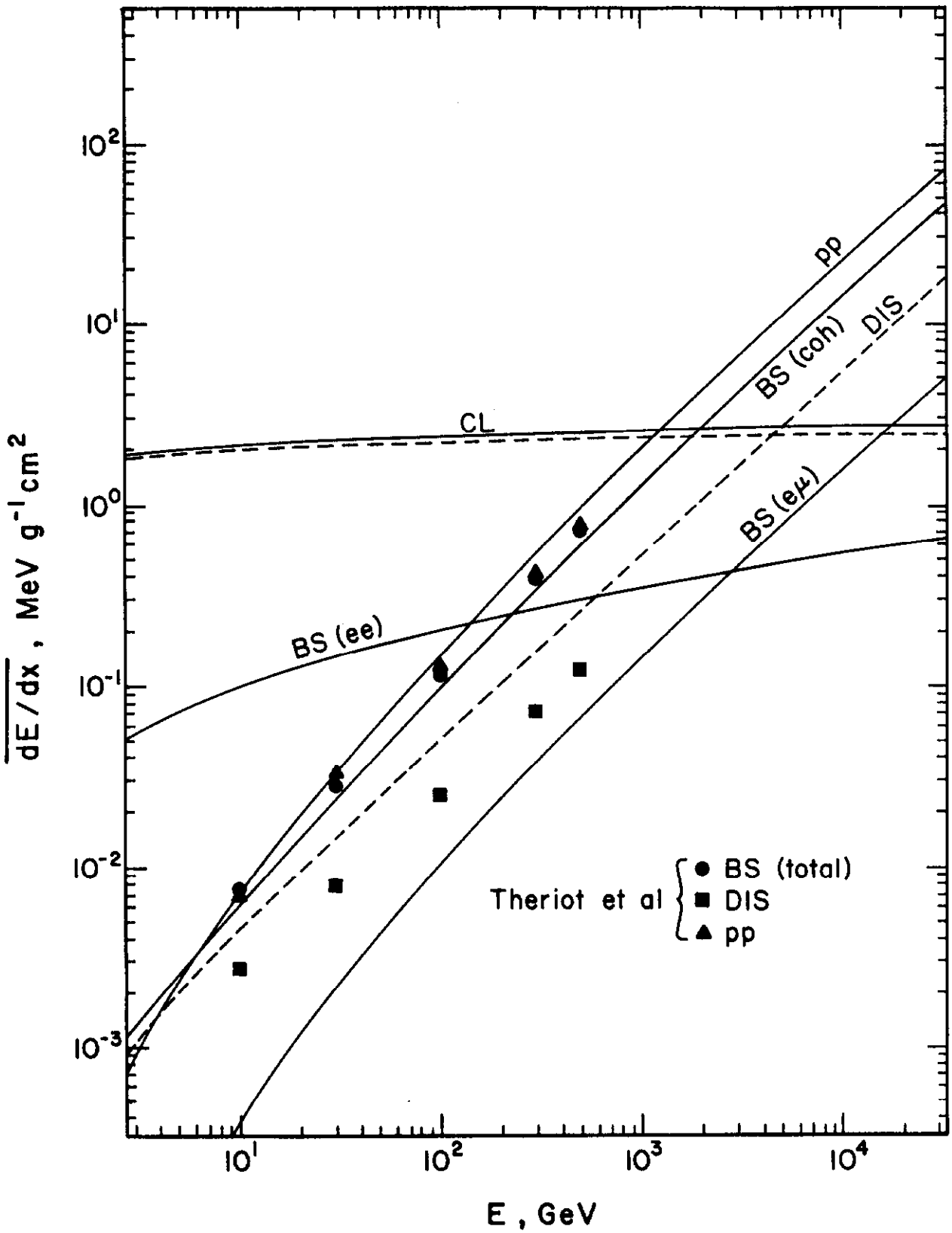
10^2
10^1
10^0
10^{-1}
10^{-2}
10^{-3}
$\overline{dE/dx}$, MeV $g^{-1}cm^2$
10^1
10^2
10^3
10^4
E , GeV
pp
BS (coh)
DIS
CL
BS (eμ)
BS (ee)
Theriot et al
BS (total)
DIS
pp

Fig. 19.a

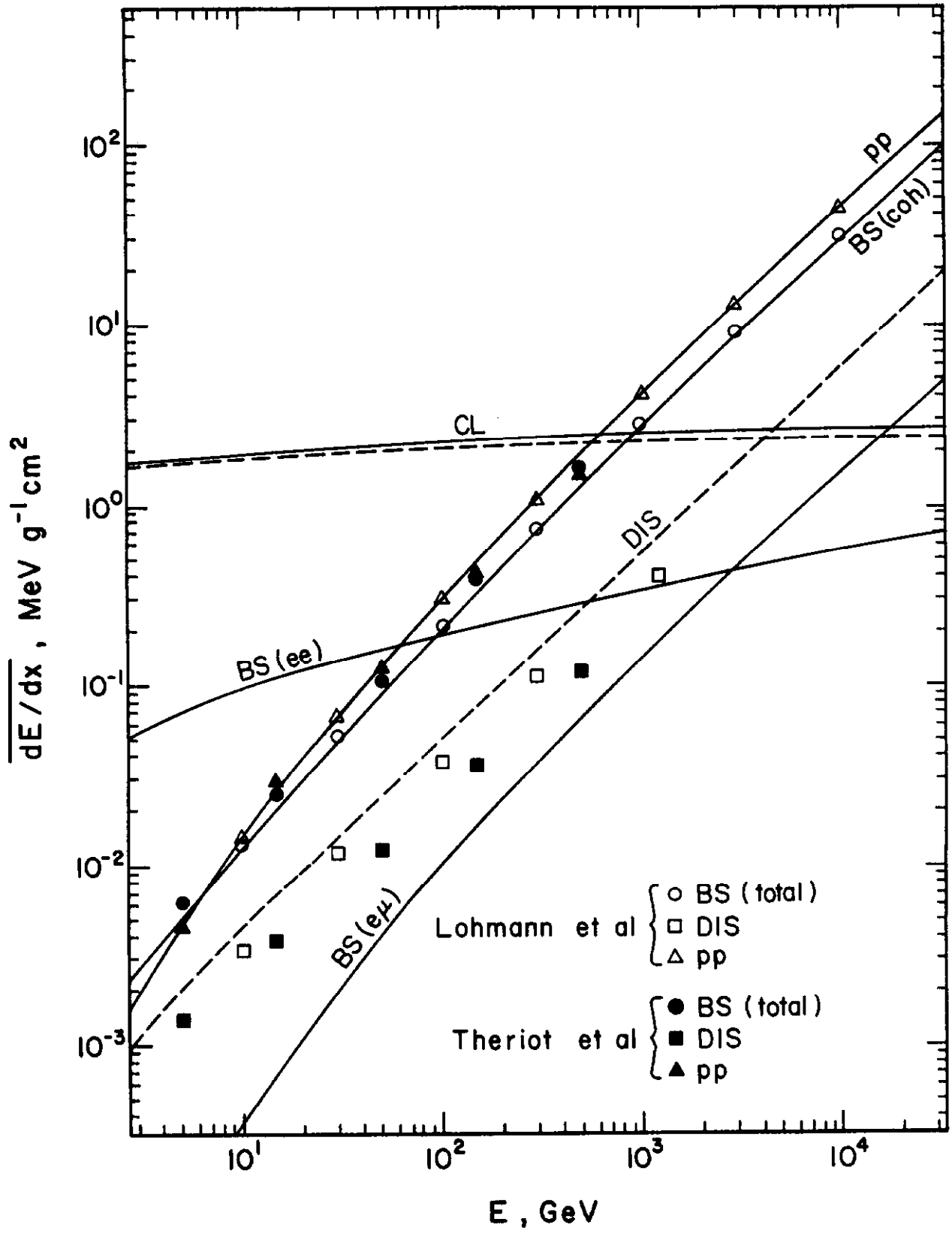
$\overline{dE/dx}$, MeV $g^{-1}cm^2$
E , GeV
pp
BS(coh)
CL
DIS
BS(ee)
BS(eμ)
Lohmann et al
BS (total)
DIS
pp
Theriot et al
BS (total)
DIS
pp

Fig. 19.b

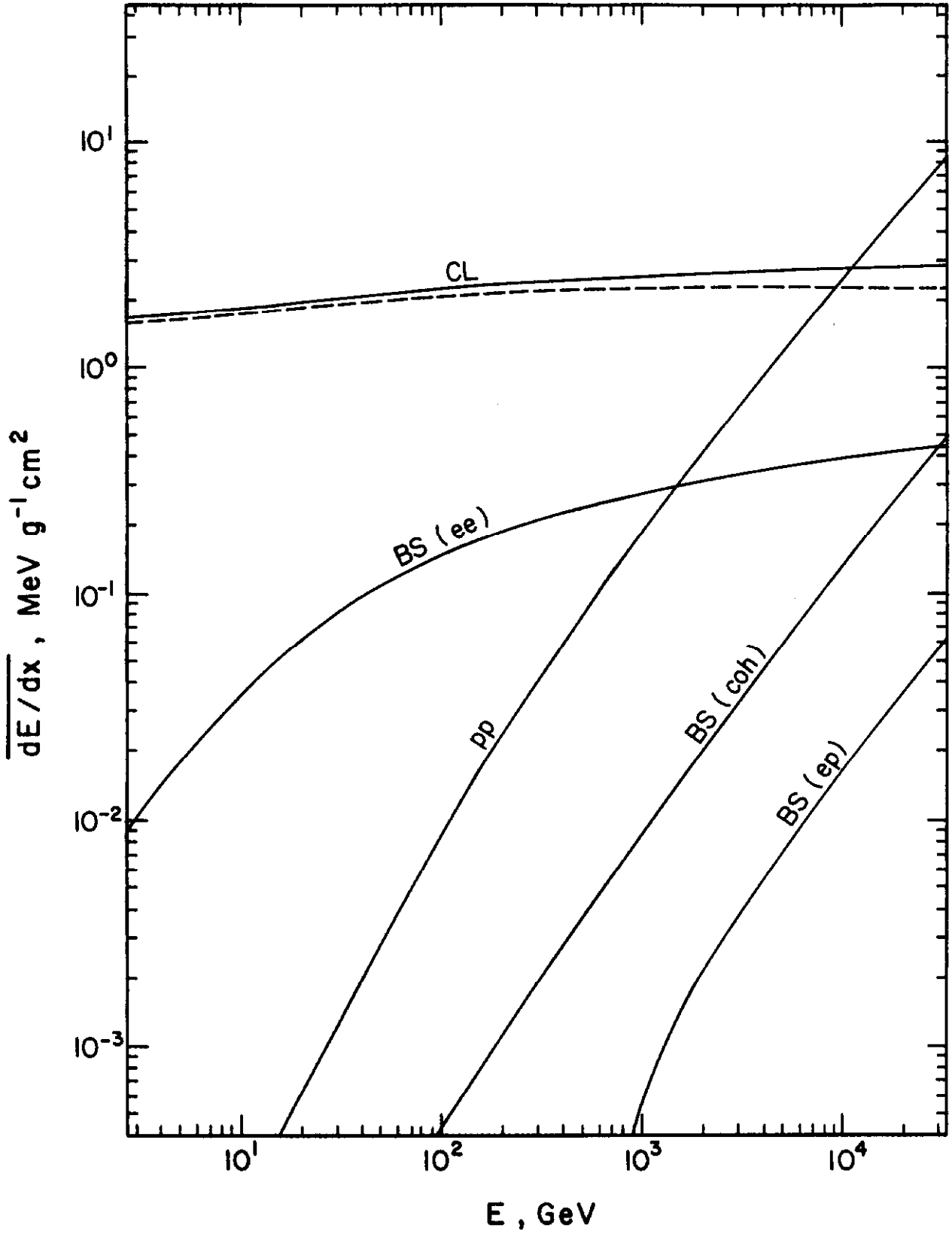
10^1
10^0
10^{-1}
10^{-2}
10^{-3}
$\overline{dE/dx}$, MeV $g^{-1}cm^2$
CL
BS (ee)
pp
BS (coh)
BS (ep)
10^1
10^2
10^3
10^4
E , GeV

Fig. 20.a

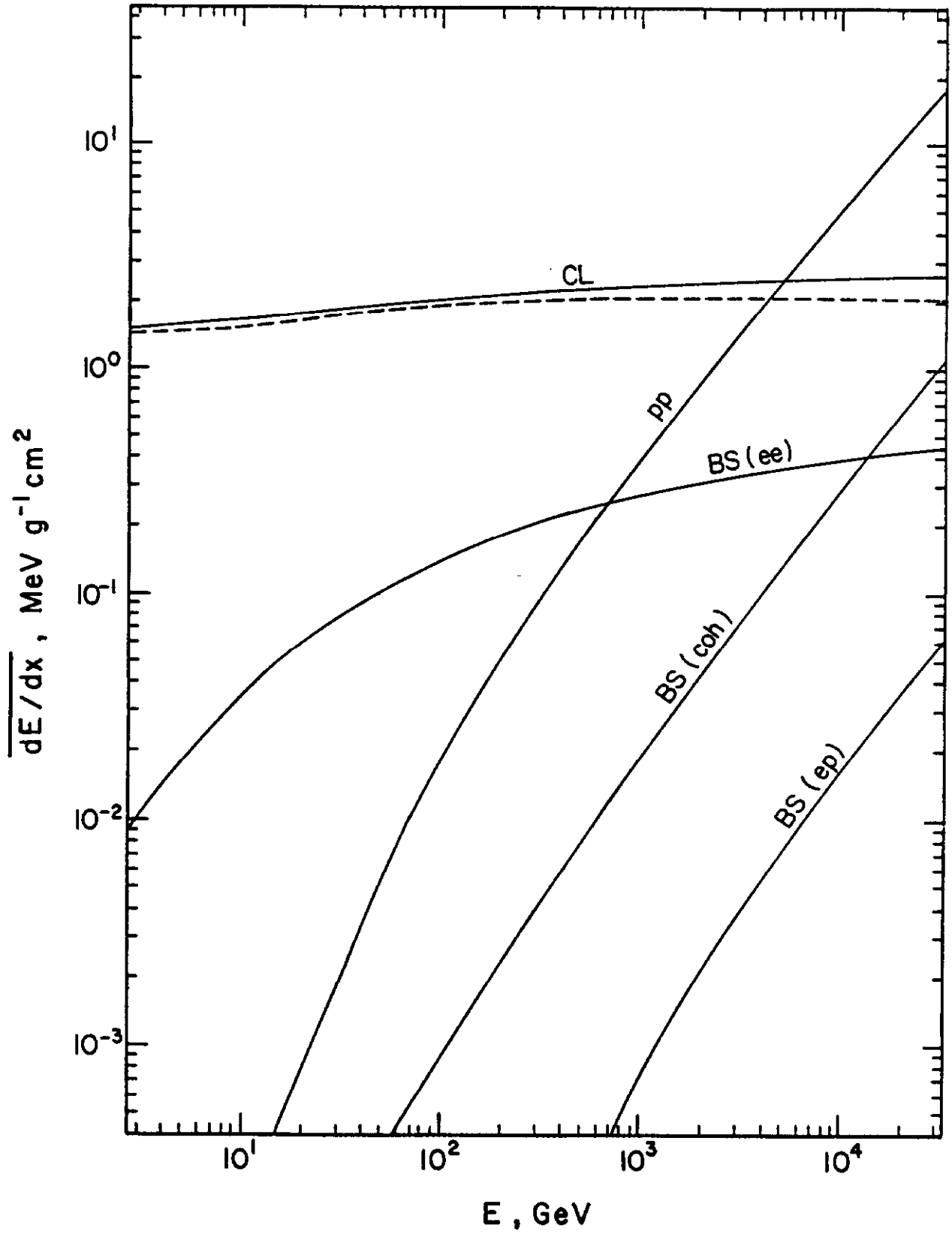
10^1
10^0
10^{-1}
10^{-2}
10^{-3}
$\overline{dE/dx}$, MeV $g^{-1}cm^2$
CL
pp
BS (ee)
BS (coh)
BS (ep)
10^1
10^2
10^3
10^4
E , GeV

Fig. 20.b

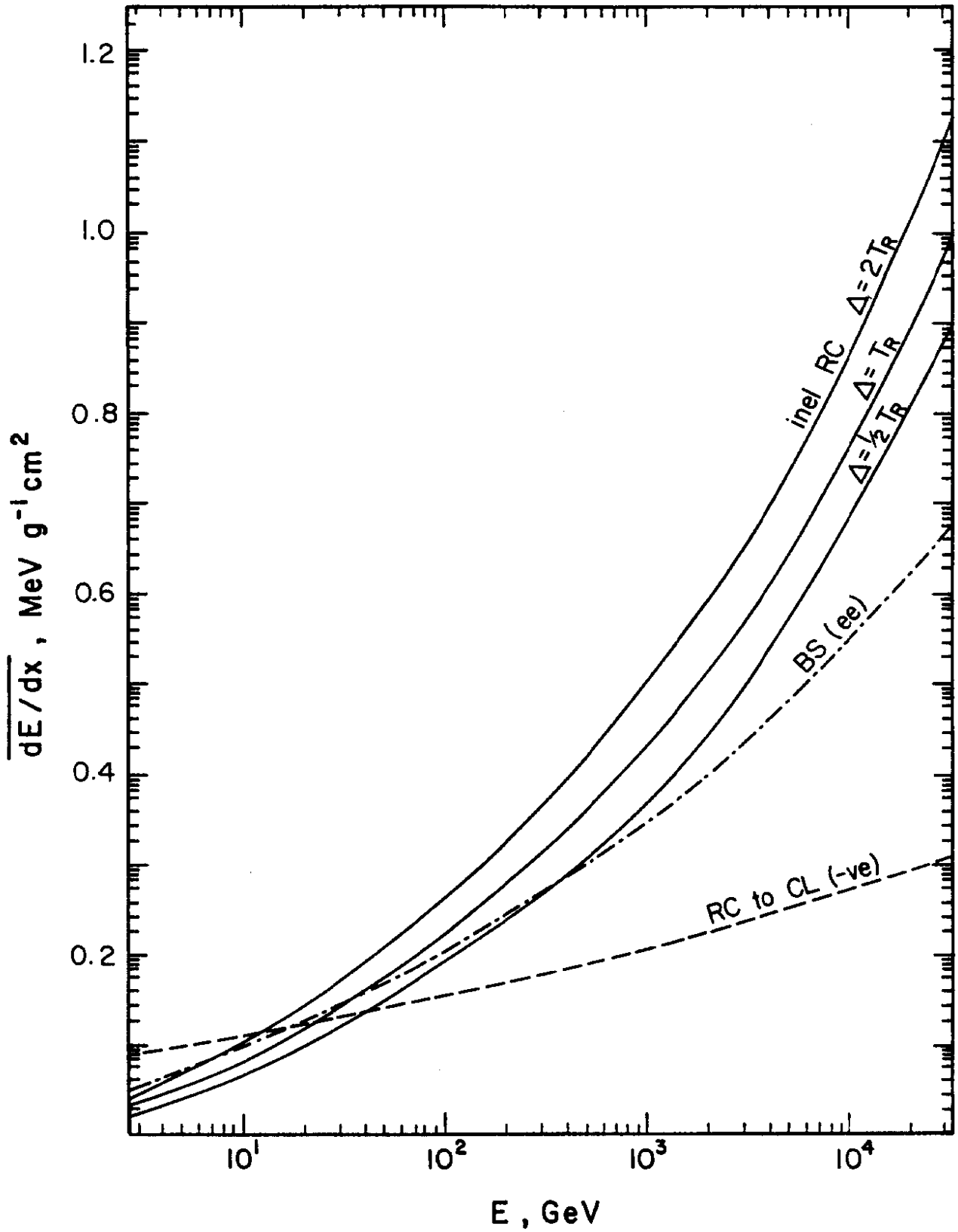
1.2
1.0
0.8
0.6
0.4
0.2
$\overline{dE/dx}$, MeV $g^{-1}cm^2$
10^1
10^2
10^3
10^4
E , GeV
inel RC
$\Delta = 2T_R$
$\Delta = T_R$
$\Delta = \frac{1}{2}T_R$
BS (ee)
RC to CL (-ve)

Fig. 21

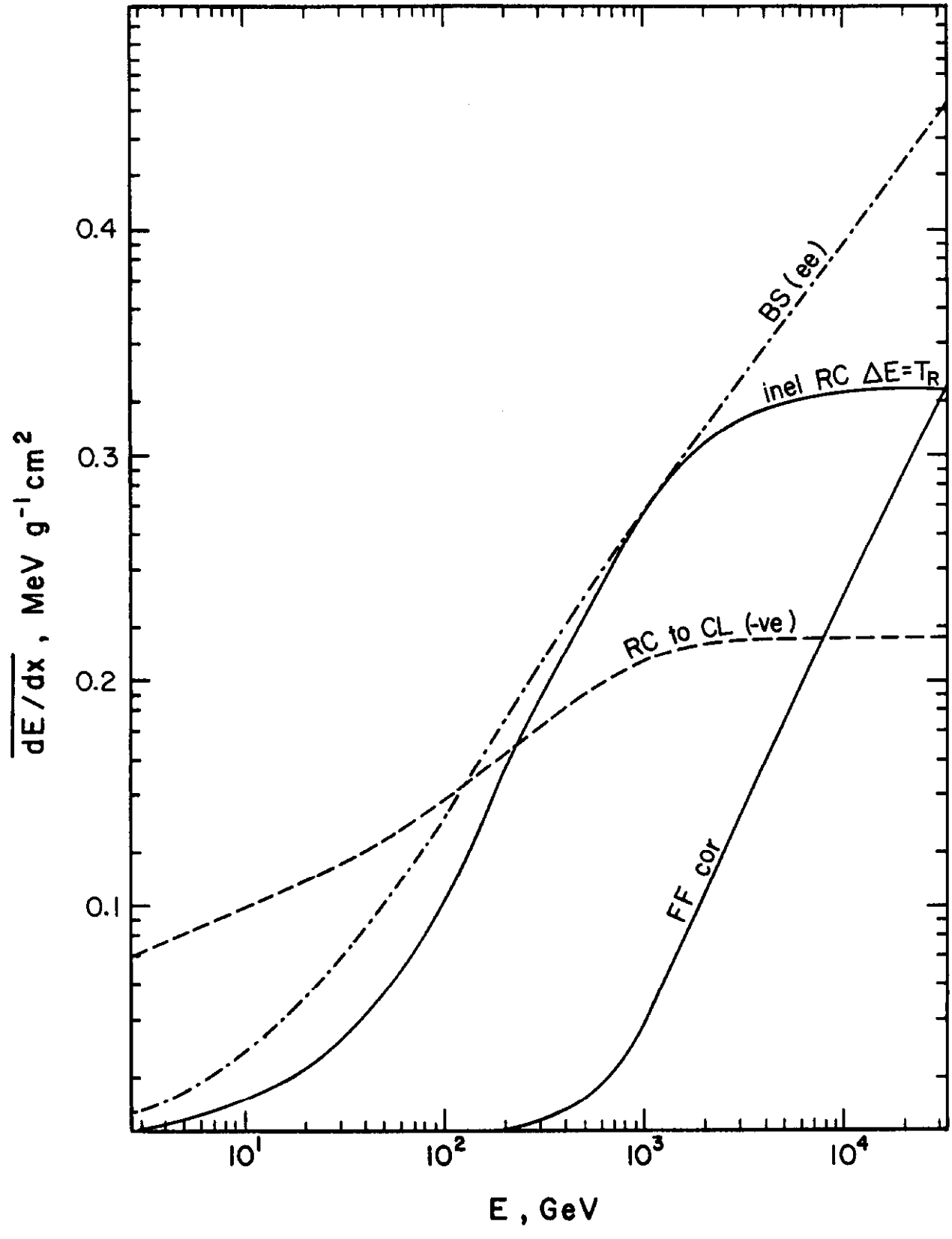
0.4
0.3
0.2
0.1
$\overline{dE/dx}$, MeV $g^{-1}cm^2$
BS (ee)
inel RC $\Delta E=T_R$
RC to CL (-ve)
FF cor
10^1
10^2
10^3
10^4
E , GeV

Fig. 22